Distributed Inter-Area Oscillation Damping Control for Power Systems by Using Wind Generators and Load Aggregators*

Zhiyuan Tang[a,*], David J. Hill[b,c], Tao Liu[b], Yue Song[b]

[a]*Department of Electrical and Computer Engineering, University of Waterloo, Canada*
[b]*Department of Electrical and Electronic Engineering, The University of Hong Kong, Hong Kong*
[c]*School of Electrical and Information Engineering, The University of Sydney, NSW 2006, Australia*

Abstract

This paper investigates the potential of wind turbine generators (WTGs) and load aggregators (LAs) to provide supplementary damping control services for low frequency inter-area oscillations (LFOs) through the additional distributed damping control units (DCUs) proposed in their controllers. In order to provide a scalable methodology for the increasing number of WTGs and LAs, a novel distributed control framework is proposed to coordinate damping controllers. Firstly, a distributed algorithm is designed to reconstruct the system Jacobian matrix for each damping bus (buses with damping controllers). Thus, the critical LFO can be identified locally at each damping bus by applying eigen-analysis to the obtained system Jacobian matrix. Then, if the damping ratio of the critical LFO is less than a preset threshold, the control parameters of DCUs will be tuned in a distributed and coordinated manner to improve the damping ratio and minimize the total control cost at the same time. The proposed control framework is tested in a modified 10-machine New England system and a modified 14-generator Australian power system. The simulation results with and without the proposed control framework are compared to demonstrate the effectiveness of the proposed framework.

Keywords: Low frequency oscillation, load-side control, wind generator, distributed control

1. Introduction

Low frequency inter-area oscillations (LFOs) have always been a matter of concern to power system operators due to their potential threats to the power system stability [1]. With the development of the electricity market and growing power demand, future power systems will become more stressed and operate closer to their stability limits, which highlights the need to improve the damping ratio of LFOs and prevent sustained oscillations that can result in serious consequences such as system separations or even large-area blackouts [1].

The power system stabilizers (PSSs) installed on conventional synchronous machines are the most important components to improve system damping against LFOs. However, the increasing penetration of wind power limits the availability of PSSs to provide sufficient damping against LFOs. For one thing, the displacement of conventional synchronous generators with wind turbine generators (WTGs) may reduce the damping ratio of inter-area modes by the reconfiguration of line power flows, reduction of system inertia, and interaction of converter controls with power system dynamics [2]. For another thing, once the conventional synchronous machines are replaced by WTGs, the associated PSSs are also removed from the system with no replacement controllers for WTGs to provide damping control services. Thus, if no new alternative controllers are developed to provide supplementary damping control services, insufficient system controls may jeopardize the system security and stability. To solve this issue, in this paper, we are looking for solutions from both the generation and load sides.

For the generation side, we utilize the converter interfaced WTGs which can provide damping torques for LFOs by quickly adjusting their active power outputs though a proper control of electronic devices that interface them with the grid [3, 4]. For the load side, the option of using highly distributed controllable loads (demand control) is appealing. Due to properties such as instantaneous responses and spatial distributions, demand control has gained a lot of attention [5, 6, 7]. In particular, demand control has been utilized to accomplish important system support tasks such as frequency control [5], voltage control [6], and small-disturbance angle stability enhancement [7]. However, the ability of demand control to provide supplementary damping control services agaist LFOs has not been thoroughly investigated yet. In this paper, the load aggregators (LAs) will be coordinated with WTGs to provide damping torques against LFOs through the additional distributed damping control units (DCUs) developed in their controllers.

*This work was fully supported by the Research Grants Council of the Hong Kong Special Administrative Region under the Theme-based Research Scheme through Project No. T23-701/14-N.

*Corresponding author
Email address: zhiyuan.tang@uwaterloo.ca (Zhiyuan Tang)

In the literature, numerous methods have been proposed to coordinate traditional damping controllers (e.g. PSS) [8, 9, 10] and new damping controllers (e.g. FACTS and HVDC) [11, 12, 13]. Approaches based on robust control theories and linear matrix inequalities (LMIs) have been utilized to deal with the uncertainties of operating conditions [9, 10, 11]. For example, in [10], the synthesis of the controller is formulated as a mixed H_2/H_∞ output feedback control problem with regional pole placement that is resolved through a linear matrix inequality approach. However, such a robust controller design method is too conservative and unable to incorporate all system constraints (e.g. hard limits on the control signals). Approaches based on model predictive control have been utilized to incorporate all system constraints. For example, the authors of [12] propose a model predictive control based HVDC supplementary controller which can incorporate plant constraints explicitly. Unfortunately, the model used in such a method is developed at a pre-given operating point, and hence, the obtained controller cannot directly guarantee robustness around the other operating points. Approaches based on fuzzy logic have been utilized to handle the variations of operating points [13]. For example, a fuzzy logic adaptive control unit is proposed in [13] to adjust control gains for different operating points. However, this fuzzy logic based method becomes very complicated when the number of damping controllers becomes large. Moreover, all the methods mentioned above are carried out in a centralized manner that lacks scalability and flexibility, i.e., a new damping controller is added into the original control system, the whole control law need to be redesigned.

To overcome the drawbacks of the abovementioned methods, in this paper, a novel distributed control framework is proposed to coordinate damping controllers, which can be implemented by local measurements and limited communications between neighboring buses. The proposed distributed control framework consists of two modules: a critical LFO identification module and a controller parameters tuning module where the communication network used in each module is different. The critical LFO identification module aims at reconstructing the system Jacobian matrix for each damping bus (a bus with damping controller, i.e., buses with WTGs or LAs) in a distributed manner where the communication network used covers all buses in the system. Thus, the critical LFO (the LFO with the least damping ratio) can be identified locally at each damping bus by applying eigen-analysis to the obtained system Jacobian matrix. Further, if the damping ratio of the critical LFO is less than a preset threshold, the parameters of DCUs will be tuned in a distributed manner to improve the damping ratio of the critical LFO and minimize the total control cost at the same time where the communication network used only covers those damping buses. The contributions of this paper are listed below:

- A novel two-step communication based distributed control framework is proposed to coordinate LAs and WTGs. The proposed control method is suitable in practice for its scalability.
- In the critical LFO identification module, based on structural properties of the original power grid, a distributed calculation algorithm is developed to recover the Jacobian matrices for each damping bus.
- In the controller parameters tuning module, based on the eigenvalue sensitivities, a controller tuning problem is formulated and solved in a distributed manner.

Compared with the robust control design (e.g., [10]), the proposed approach has the following three advantages. The first one is the low calculation cost involved in the controller parameter tuning process. For the robust design (e.g., [10]), the tuning process is handled by solving large-size LMIs, while in this approach, only a small-size convex optimization problem is involved. The second advantage comes from the improved control accuracy. In our approach, the control effect of each controller is assessed based on the current operating condition, which is used to determine the best coordination among controllers. In other words, the proposed approach can fully exploit the control potential of controllers under different operating conditions, whereas in the robust design, the control settings are fixed and conservative since they are designed over a wide range of possible operating conditions. The third advantage is the improved scalability. For a centralized robust method, when a new controller is added in the network, it has to be redesigned [8]. While for the proposed distributed approach, a new controller can take part in the control process as long as it has the ability of data processing and communicating with at least one existed controller [14].

The rest of the paper is organized as follows. Section 2 introduces the DCU and the power system model to be studied. The proposed distributed control framework is explicitly presented in Section 3. Section 4 presents a case study by using a modified 10-machine New England system and a modified 14-generator Australian power system. Conclusions are given in Section 5.

Notations

Denote $\mathbb{R}$ and $\mathbb{C}$ as the set of real numbers and complex numbers, respectively. An m-dimensional vector is denoted as $\boldsymbol{x} = [x_i] \in \mathbb{R}^m$. The transpose of a vector or a matrix is defined as $(\cdot)^T$. The notation $\boldsymbol{I}_m \in \mathbb{R}^{m\times m}$ denotes the identity matrix, $\mathbf{0}$ is a zero vector or matrix with an appropriate dimention, and $\boldsymbol{e}_i \in \mathbb{R}^p$ denotes the vector with the i^{th} entry being one and others being zeros. The notation $|x|$ ($\angle x$) takes the modulus (angle) of a complex number $x \in \mathbb{C}$. The notation $\mathbb{V}(\boldsymbol{A})$ means converting the matrix $\boldsymbol{A} = [\boldsymbol{a}_1, \ldots, \boldsymbol{a}_p] \in \mathbb{R}^{m\times p}$ with $\boldsymbol{a}_i \in \mathbb{R}^m$ with $i = 1, \ldots, p$ to a vector, i.e., $\mathbb{V}(\boldsymbol{A}) = [\boldsymbol{a}_1^T, \ldots, \boldsymbol{a}_p^T]^T \in \mathbb{R}^{mp}$.

The symbols $\|\cdot\|$ and $\|\cdot\|_\infty$ denote the l_2 and l_∞ norms for a vector, respectively.

2. Network Description

In this section, we firstly introduce the DCU proposed for each damping controller (i.e., WTGs and LAs). Then, the power system network to be studied is introduced, which will be used to design the control framework in Section 3.

2.1. Distributed Damping Control Unit

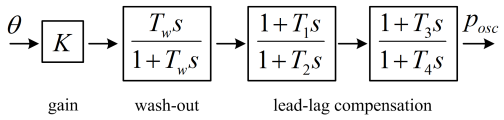

Figure 1: The control block diagram of the proposed DCU.

Fig. 1 shows the block diagram of the proposed DCU which mimics the structure of PSS. The input is the local bus voltage angle θ_i that is defined as the angle difference with respect to a synchronously rotating reference. The output is p_{osci} which is added to the reference active power demand of the WTG or LA to provide supplementary damping control services. The mathematical model of the i^{th} DCU is given by

$$\begin{aligned}
\dot{x}_{1i} &= -\frac{1}{T_{wi}}\left(K_i\theta_i + x_{1i}\right)\\
\dot{x}_{2i} &= \frac{1}{T_{2i}}\left((1-\frac{T_{1i}}{T_{2i}})(K_i\theta_i + x_{1i}) - x_{2i}\right)\\
\dot{x}_{3i} &= \frac{1}{T_{4i}}\left((1-\frac{T_{3i}}{T_{4i}})\left(x_{2i} + \left(\frac{T_{1i}}{T_{2i}}(K_i\theta_i + x_{1i})\right)\right) - x_{3i}\right)\\
p_{osci} &= x_{3i} + \frac{T_{3i}}{T_{4i}}\left(x_{2i} + \frac{T_{1i}}{T_{2i}}(K_i\theta_i + x_{1i})\right).
\end{aligned} \tag{1}$$

The dynamics can be written in a compact form as $\dot{\boldsymbol{x}}_{Ci} = \boldsymbol{f}_{Ci}(\boldsymbol{x}_{Ci}, \theta_i)$ where $\boldsymbol{x}_{Ci} = [x_{1i}, x_{2i}, x_{3i}]^T$ is the supplementary state variables, K_i is the gain, T_{wi} is the wash-out time constant, T_{1i}, T_{2i}, T_{3i}, and T_{4i} are time constants for lead-lag compensation. In the proposed control framework, K_i, T_{1i}, T_{2i}, T_{3i}, and T_{4i} will be tuned to improve the damping ratio of the critical LFO. It will be shown in the case study (Fig. 11) that the introduction of DCU has an impact on the existed weak oscillation modes, but will not create new weak modes.

Fig. 2 shows the implementation of DCU on each damping controller (i.e., WTG and LA). In this paper, we consider the active power modulation for supplementary damping proposes, i.e., the output of each DCU p_{osci} is added to the reference active power demand of the WTG or LA p_{refi} to create new reference demand $p^\star_{refi}$. In order to avoid an excessive interference of the normal operation of WTGs and LAs, as did in [15, 16], the output of each DCU p_{osci} is limited by the range $[p^{min}_{osci}, p^{max}_{osci}]$ which is usually selected as ± 5 % p.u. [16].

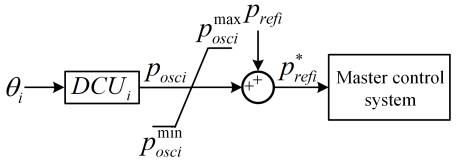

Figure 2: Schematic of DCU's implementation.

2.2. Power system network

Consider a connected power system consisting of N buses with N_G synchronous generators (SGs), N_W WTGs, N_L loads, and N_T transfer buses where $N = N_G + N_W + N_L + N_T$. The SG (WTG or load) bus refers to a bus that connects a SG (WTG or load) only. The transfer bus is a bus with no generation or demand. We number the SG buses as $\mathcal{V}_G = \{1, \ldots, N_G\}$, WTG buses as $\mathcal{V}_W = \{N_G+1, \ldots, N_G+N_W\}$, load buses as $\mathcal{V}_L = \{N_G + N_W + 1, \ldots, N_G + N_W + N_L\}$, and transfer buses as $\mathcal{V}_T = \{N_G+N_W+N_L+1, \ldots, N\}$. In order to make WTGs and LAs provide supplementary damping control services, we assume that each WTG (LA) has a DCU.

2.2.1. SG model

To highlight the effectiveness of the proposed damping controllers, PSSs are not included in the SG models. With the 4^{th}-order two-axis synchronous machine model and IEEE standard exciter model (IEEET1), the mathematical model of the i^{th} SG is written as:

$$\begin{aligned}
\dot{\boldsymbol{x}}_{Gi} &= \boldsymbol{f}_{Gi}(\boldsymbol{x}_{Gi}, \theta_i, v_i)\\
p_{Gi} &= g_{p_{Gi}}(\boldsymbol{x}_{Gi}, \theta_i, v_i)\\
q_{Gi} &= g_{q_{Gi}}(\boldsymbol{x}_{Gi}, \theta_i, v_i),\ i \in \mathcal{V}_G
\end{aligned} \tag{2}$$

where the state variable $\boldsymbol{x}_{Gi}$ is defined as $\boldsymbol{x}_{Gi} = [e'_{qi}, e'_{di}, \delta_i, \omega_i, x_{mi}, x_{r1i}, x_{r2i}, x_{fi}]^T$; e'_{qi} and e'_{di} are transient d-axis and q-axis voltages, respectively; δ_i and ω_i are the rotor angle and speed, respectively; x_{mi}, x_{r1i}, x_{r2i} and x_{fi} are the state variables corresponding to the IEEET1 exciter. The algebraic variables are the local bus voltage angle θ_i and magnitude v_i. The active and reactive power injections of the i^{th} SG bus are denoted as p_{Gi} and q_{Gi}, respectively. The detailed descriptions of nonlinear functions $\boldsymbol{f}_{Gi}$, $g_{p_{Gi}}$, $g_{q_{Gi}}$ can be found in [17], which is also given in Appendix 6.1 for completeness.

2.2.2. WTG model

A wind farm may consist of hundreds of wind turbines. It is difficult and unnecessary to model each individual unit in a wind farm for large system studies. In this work, a large WTG model is employed to represent an equivalent

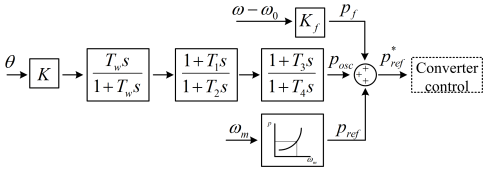

Figure 3: Control block diagram of the controller for WTG.

lumped model of a wind farm, which has been widely used in the literature (e.g., [16, 18]). For the WTG model, fully rated converter (FRC) WTGs are adopted, which employ the configuration of a synchronous machine with a permanent magnet rotor [18]. Normally, the controller of WTG gives a reference active power demand to optimize the wind energy capture based on the measured rotor speed (see the lower branch in Fig. 3). In this paper, two additional control units are added into the original WTG's controller to adapt the active power reference set point, i.e., the primary frequency support unit proposed in [19] (see the upper branch in Fig. 3) and the DCU (see the middle branch in Fig. 3). It is assumed that a small portion of active power capacity (e.g. 5%) is reserved by each WTG for damping control support and primary frequency support [19]. The mathematical model of the i^{th} WTG is written as:

$$\begin{aligned} \dot{\theta}_i &= \omega_i \\ \dot{\boldsymbol{x}}_{Wi} &= \boldsymbol{f}_{Wi}(\boldsymbol{x}_{Wi}, \omega_i, \theta_i, v_i) \\ p_{Wi} &= g_{p_{Wi}}(\boldsymbol{x}_{Wi}, \omega_i, \theta_i, v_i) \\ q_{Wi} &= g_{q_{Wi}}(\boldsymbol{x}_{Wi}, \omega_i, \theta_i, v_i),\ i \in \mathcal{V}_W \end{aligned} \tag{3}$$

where ω_i denotes the local bus frequency that is the frequency deviation from the nominal value. If the system is (not) in steady state, the local bus frequencies of different buses are the same (can be different). The state variable $\boldsymbol{x}_{Wi} = [\omega_{mi}, \theta_{pi}, i_{sqi}, i_{cdi}, \boldsymbol{x}_{Ci}^T]^T$ where ω_{m_i} is the rotor speed; θ_{p_i} is the pitch angle used for maximum power control; i_{qsi} is the generator stator quadrature current used for active power/speed control; and i_{cdi} is the converter direct current used for reactive power/voltage control; $\boldsymbol{x}_{Ci} = [x_{1i}, x_{2i}, x_{3i}]^T$ are state variables corresponding to the DCU. The active and reactive power injections of the i^{th} WTG bus are denoted as p_{Wi} and q_{Wi}, respectively. The detailed descriptions of nonlinear functions $\boldsymbol{f}_{Wi}$, $g_{p_{Wi}}$, $g_{q_{Wi}}$ are given in Appendix 6.2.

2.2.3. Load model

The active power of each load p_{Li} is divided into two parts: the controllable part $d_i = p_{osci}(\boldsymbol{x}_{Li}, \theta_i)$ (referred to as LA in this paper) and static voltage frequency dependent part, whereas the reactive power of each load q_{Li} is assumed to be static voltage frequency dependent. For the LA at each load bus, we assume that it controls a group of small controllable loads (e.g. electric springs in distribution networks [20]) that can change their power consumptions very quickly via the electronic interface. In this way, each LA can provide the active power change (i.e., reserve capacity) required for damping control via the introduced DCU. With the additional DCU, the mathematical model of the i^{th} load bus is given as follows:

$$\begin{aligned} \dot{\theta}_i =& \omega_i \\ \dot{\boldsymbol{x}}_{Li} =& \boldsymbol{f}_{Li}(\boldsymbol{x}_{Li}, \theta_i) \\ p_{Li} =& p_{oi}(v_i)^{\alpha_i}(1 + k_{pfi}(\omega_i - \omega_0)) + d_i(\boldsymbol{x}_{Li}, \theta_i) \\ :=& g_{p_{Li}}(\boldsymbol{x}_{Li}, \omega_i, \theta_i, v_i) \\ q_{Li} =& q_{o_i}(v_i)^{\beta_i}(1 + k_{qf_i}(\omega_i - \omega_0)) \\ :=& g_{q_{Li}}(\omega_i, v_i),\ i \in \mathcal{V}_L \end{aligned} \tag{4}$$

where p_{oi} and q_{oi} are the nominal values; α_i and β_i are voltage coefficients; and k_{pfi} and k_{qfi} are frequency coefficients. The state variable $\boldsymbol{x}_{Li} = [x_{1i}, x_{2i}, x_{3i}]^T$ corresponds to the DCU, which introduce the dynamics of the load model.

2.2.4. Transfer bus

As transfer buses have no generations or loads, the i^{th} transfer bus is simply modeled as:

$$p_{Ti} = 0,\ q_{Ti} = 0,\ i \in \mathcal{V}_T \tag{5}$$

where p_{Ti} and q_{Ti} are the active and reactive power injections, respectively.

2.2.5. Network power flows

The network power flows are represented by the usual set of algebraic power flow equations, which are used to couple all buses power injection equations mentioned above. For the i^{th} bus in the system, the power flow equations are given as:

$$\begin{aligned} 0 &= -p_i^{inj} + v_i \sum_{j=1}^{N} v_j (G_{ij} \cos\theta_{ij} + B_{ij} \sin\theta_{ij}) \\ 0 &= -q_i^{inj} + v_i \sum_{j=1}^{N} v_j (G_{ij} \sin\theta_{ij} - B_{ij} \cos\theta_{ij}),\ i \in \mathcal{V} \end{aligned} \tag{6}$$

where G_{ij} and B_{ij} are the real and imaginary parts of Y_{ij} which is the (i, j) entry of the admittance matrix $\boldsymbol{Y}$; the notation θ_{ij} is the short for $\theta_i - \theta_j$; the set $\mathcal{V} = \mathcal{V}_G \cup \mathcal{V}_W \cup \mathcal{V}_L \cup \mathcal{V}_T$; p_i^{inj} and q_i^{inj} are injected active and reactive power of the i^{th} bus, respectively. In particular, for SG buses, $p_i^{inj} = p_{Gi}$ and $q_i^{inj} = q_{Gi}$; for WTG buses, $p_i^{inj} = p_{Wi}$ and $q_i^{inj} = q_{Wi}$; for load buses, $p_i^{inj} = -p_{Li}$ and $q_i^{inj} = -q_{Li}$; and for transfer buses, $p_i^{inj} = p_{Ti}$ and $q_i^{inj} = q_{Ti}$.

2.2.6. Overall system

Combining (2)-(6), the overall system can be expressed as differential-algebraic equations:

$$\begin{aligned} \dot{\boldsymbol{x}} &= \boldsymbol{f}(\boldsymbol{x}, \boldsymbol{y}) \\ \boldsymbol{0} &= \boldsymbol{h}(\boldsymbol{x}, \boldsymbol{y}) \end{aligned} \tag{7}$$

where the vector $\boldsymbol{x} = [\boldsymbol{x}_G^T, \boldsymbol{\theta}_W^T, \boldsymbol{x}_W^T, \boldsymbol{\theta}_L^T, \boldsymbol{x}_L^T]^T$ and the vector $\boldsymbol{y} = [\boldsymbol{\theta}_G^T, \boldsymbol{\omega}_W^T, \boldsymbol{\omega}_L^T, \boldsymbol{\theta}_T^T, \boldsymbol{v}_G^T, \boldsymbol{v}_W^T, \boldsymbol{v}_L^T, \boldsymbol{v}_T^T]^T$; $\boldsymbol{x}_k = [\boldsymbol{x}_{k1}^T, \ldots, \boldsymbol{x}_{ki}^T, \ldots, \boldsymbol{x}_{kN_k}^T]^T,\ i \in \mathcal{V}_k,\ k \in \{G, W, L\}$; $\boldsymbol{\theta}_k = [\theta_i] \in \mathbb{R}^{N_k},\ i \in \mathcal{V}_k,\ k \in \{G, W, L, T\}$; $\boldsymbol{v}_k = [v_i] \in \mathbb{R}^{N_k},\ i \in \mathcal{V}_k,\ k \in \{G, W, L, T\}$; $\boldsymbol{\omega}_k = [\omega_i] \in \mathbb{R}^{N_k},\ i \in \mathcal{V}_k,\ k \in \{W, L\}$. The nonlinear functions $\boldsymbol{f}$ and $\boldsymbol{h}$ represent the system dynamics and network power flow equations, respectively, where $\boldsymbol{f} = [\boldsymbol{f}_S^T, \boldsymbol{f}_{\omega C}^T, \boldsymbol{f}_C^T, \boldsymbol{f}_{\omega L}^T, \boldsymbol{f}_L^T]^T$ and $\boldsymbol{h} = [\boldsymbol{h}_{pS}^T, \boldsymbol{h}_{pC}^T, \boldsymbol{h}_{pL}^T, \boldsymbol{h}_{qS}^T, \boldsymbol{h}_{qC}^T, \boldsymbol{h}_{qL}^T]^T$ which are component-wise (the component function $h_{p_{S_i}} \coloneqq g_{p_{S_i}} - p_i^{inj},\ i \in \mathcal{V}_S$; $h_{p_{C_i}} \coloneqq g_{p_{C_i}} - p_i^{inj},\ i \in \mathcal{V}_C$; $h_{p_{L_i}} \coloneqq g_{p_{L_i}} + p_i^{inj},\ i \in \mathcal{V}_L$; $h_{q_{S_i}} \coloneqq g_{q_{S_i}} - q_i^{inj},\ i \in \mathcal{V}_S$; $h_{q_{C_i}} \coloneqq g_{q_{C_i}} - q_i^{inj},\ i \in \mathcal{V}_C$; and $h_{q_{L_i}} \coloneqq g_{q_{L_i}} + q_i^{inj},\ i \in \mathcal{V}_L$).

Linearizing system (7) gives the following linear model:

$$\left[\begin{array}{c} \Delta\dot{\boldsymbol{x}} \\ \hdashline \boldsymbol{0} \end{array}\right] = \left[\begin{array}{c:c} \boldsymbol{A}_s & \boldsymbol{B}_s \\ \hdashline \boldsymbol{C}_s & \boldsymbol{D}_s \end{array}\right] \left[\begin{array}{c} \Delta\boldsymbol{x} \\ \hdashline \Delta\boldsymbol{y} \end{array}\right] \tag{8}$$

where the detailed expressions of the matrices $\boldsymbol{A}_s$, $\boldsymbol{B}_s$, $\boldsymbol{C}_s$, and $\boldsymbol{D}_s$ are given in Appendix 6.3. Assuming $\boldsymbol{D}_s$ is nonsingular (it is a common assumption adopted in the literature [14]) and eliminating $\Delta\boldsymbol{y}$ in (8) gives:

$$\Delta\dot{\boldsymbol{x}} = \boldsymbol{A}_r \Delta\boldsymbol{x} \tag{9}$$

where $\boldsymbol{A}_r = \boldsymbol{A}_s - \boldsymbol{B}_s \boldsymbol{D}_s^{-1} \boldsymbol{C}_s \in \mathbb{R}^{N_A \times N_A}$ with $N_A = 8N_G + 8N_W + 4N_L$.

Remark 1. *In this work, we assume that there are DCUs available at load and WTG buses which are used to provide the supplementary damping control services. This assumption is not unreasonable for future power systems since 1) both WTGs and loads can change their power outputs quickly thanks to the development of advanced electronic devices (e.g., full converter wind turbines [18] and electric springs [20]) and 2) the proposed control block can be embedded into their main control loops without increasing the complexity of the device [21, 22]. Although the aggregate load (i.e., LA) and lumped wind farm model (i.e., WTG) are employed for study, it is worth mentioning that the responses of LAs and WTGs can serve as the reference signals to the group of individual control devices controlled by them (e.g., electric springs in distribution networks or wind turbines in a wind farm) [5]. Then, the problem becomes how to make the hundreds or thousands of control devices work together to follow the reference signal. This new problem deserves attention and will be studied in future.*

3. Distributed Control Framework

With the proposed DCUs described in Section 2, LAs and WTGs can provide supplementary damping control services. In order to coordinate LAs and WTGs properly, a novel distributed control framework is proposed in this work. The proposed framework consists of two modules: the critical LFO identification module and controller parameters tuning module. In this section, based on the system model described in Section 2, these two modules will be introduced in details.

3.1. Critical LFO identification module

As mentioned earlier, this module aims at identifying the critical LFO for each damping bus in a distributed manner. It is known that the critical LFO can be investigated by applying eigenvalue analysis based on the global information, i.e., the system Jacobian matrix $\boldsymbol{A}_r$ in (9) which is usually obtained in a centralized manner [1]. However, in this paper, we will reconstruct the matrix $\boldsymbol{A}_r$ for each damping bus in a distributed manner by revealing the structure properties of the power grid contained in the matrices $\boldsymbol{A}_s$, $\boldsymbol{B}_s$, $\boldsymbol{C}_s$, and $\boldsymbol{D}_s$.

By performing an elementary column operation, the matrices $\boldsymbol{A}_s$, $\boldsymbol{B}_s$, $\boldsymbol{C}_s$, and $\boldsymbol{D}_s$ can be reformulated as:

$$\left[\begin{array}{c:c} \boldsymbol{A}_s & \boldsymbol{B}_s \\ \hdashline \boldsymbol{C}_s & \boldsymbol{D}_s \end{array}\right] = \left[\begin{array}{c:c} \boldsymbol{K}_1 & \boldsymbol{K}_2 \\ \hdashline \boldsymbol{K}_3 & \boldsymbol{J}_{pf} \end{array}\right] \boldsymbol{T} \tag{10}$$

where the matrix $\boldsymbol{T}$ is the elementary column operator and $\boldsymbol{J}_{pf}$ is the power flow Jacobian matrix. The detailed expressions of the matrices $\boldsymbol{T}$, $\boldsymbol{K}_1$, $\boldsymbol{K}_2$, $\boldsymbol{K}_3$, and $\boldsymbol{J}_{pf}$ are given in Appendix 6.3.

Through the matrix transform (10), we can see that the matrices $\boldsymbol{A}_s$, $\boldsymbol{B}_s$, $\boldsymbol{C}_s$, and $\boldsymbol{D}_s$ can be reconstructed by all Jacobian matrices $\boldsymbol{K}_{\boldsymbol{x}_j}^{\boldsymbol{f}_i}$, $\boldsymbol{K}_{\boldsymbol{x}_j}^{\boldsymbol{h}_i}$, $\boldsymbol{J}_{pf}$ (refer to (52) for details), identity matrices, and $\boldsymbol{T}$. For identity matrices and $\boldsymbol{T}$, since they are constant, they can be broadcasted or stored at each damping bus in advance. For all Jacobian matrices $\boldsymbol{K}_{\boldsymbol{x}_j}^{\boldsymbol{f}_i}$, $\boldsymbol{K}_{\boldsymbol{x}_j}^{\boldsymbol{h}_i}$ (which all are block diagonal matrices and expressed as $\boldsymbol{K}_{\diamondsuit}^{\diamondsuit}$ hereinafter for convenience) and $\boldsymbol{J}_{pf}$, we adopt the distributed algorithm proposed in [14] that has total $2N$ steps to calculate their elements, where the communication network used covers all buses in the system and has the same topology as the physical grid. The communication network can be described by the undirected graph $\mathcal{G}_1 = \{\mathcal{V}, \mathcal{E}\}$, where $\mathcal{V}$ is the set of nodes (buses) and $\mathcal{E} \subseteq \mathcal{V} \times \mathcal{V}$ represents the set of edges (branches). The set of neighbors of node i is represent by $\mathcal{N}_i = \{j \in \mathcal{V} : (j, i) \in \mathcal{E}\}$ with cardinality $|\mathcal{N}_i| = \mathcal{D}_i$. We assume that 1) each bus knows the parameters of its local machine (or load) and lines connecting it; 2) each damping bus knows the model structure of SG, WTG, and load; 3) each bus knows its own bus number and total number of buses N; 4) each bus in the system has the capability of local measurement, storing data, processing data, communicating with its neighbors, and calculation; and 5) communication delays are negligible.

At each step, bus $i,\ i \in \mathcal{V}$ has four columns of data for communication, denoted as $\boldsymbol{\gamma}_i^a$, $\boldsymbol{\varpi}_i^a$, $\boldsymbol{\gamma}_i^b$, $\boldsymbol{\varpi}_i^b \in \mathbb{R}^{2N}$. The data update process is designed as follows:

$$[\boldsymbol{X}^a(\tau+1), \boldsymbol{X}^b(\tau+1)] = \boldsymbol{J}_{pf}[\boldsymbol{X}^a(\tau), \boldsymbol{X}^b(\tau)] \tag{11}$$

where $\boldsymbol{X}^a(\tau),\ \boldsymbol{X}^b(\tau) \in \mathbb{R}^{2N\times 2N}$ are the data matrices at the τ^{th} step iteration with the definitions as follows:

$$\begin{aligned}\boldsymbol{X}^a(\tau) &= [\boldsymbol{\gamma}_1^a(\tau),\ldots,\boldsymbol{\gamma}_N^a(\tau),\boldsymbol{\varpi}_1^a(\tau),\ldots,\boldsymbol{\varpi}_N^a(\tau)]^T\\ \boldsymbol{X}^b(\tau) &= [\boldsymbol{\gamma}_1^b(\tau),\ldots,\boldsymbol{\gamma}_N^b(\tau),\boldsymbol{\varpi}_1^b(\tau),\ldots,\boldsymbol{\varpi}_N^b(\tau)]^T\end{aligned} \tag{12}$$

which are initialized by $\boldsymbol{X}^a(0)=\boldsymbol{I}_{2N}$ and $\boldsymbol{X}^b(0)=[\boldsymbol{\gamma}_1^b(0),\ldots,\boldsymbol{\gamma}_N^b(0),\boldsymbol{\varpi}_1^b(0),\ldots,\boldsymbol{\varpi}_N^b(0)]^T$. The vectors $\boldsymbol{\gamma}_i^b(0)$ and $\boldsymbol{\varpi}_i^b(0)$ assigned to the i^{th} bus satisfies:

$$\begin{aligned}[\boldsymbol{\gamma}_i^b(0);\boldsymbol{\varpi}_i^b(0)] = [&\mathbb{V}(\boldsymbol{K}_{\boldsymbol{x}_{Gi}}^{\boldsymbol{f}_{Gi}});\mathbb{V}(\boldsymbol{K}_{\boldsymbol{\theta}_i}^{\boldsymbol{f}_{Gi}});\mathbb{V}(\boldsymbol{K}_{\boldsymbol{v}_i}^{\boldsymbol{f}_{Gi}});\\ &\mathbb{V}(\boldsymbol{K}_{\boldsymbol{x}_{Gi}}^{\boldsymbol{h}_{p_{Gi}}});\mathbb{V}(\boldsymbol{K}_{\boldsymbol{x}_{Gi}}^{\boldsymbol{h}_{q_{Gi}}});\boldsymbol{0}],\ i\in\mathcal{V}_G;\end{aligned} \tag{13a}$$

$$\begin{aligned}[\boldsymbol{\gamma}_i^b(0);\boldsymbol{\varpi}_i^b(0)] = [&\mathbb{V}(\boldsymbol{K}_{\boldsymbol{\theta}_i}^{\boldsymbol{f}_{Wi}});\mathbb{V}(\boldsymbol{K}_{\boldsymbol{x}_{Wi}}^{\boldsymbol{f}_{Wi}});\mathbb{V}(\boldsymbol{K}_{\boldsymbol{\omega}_i}^{\boldsymbol{f}_{Wi}});\\ &\mathbb{V}(\boldsymbol{K}_{\boldsymbol{v}_i}^{\boldsymbol{f}_{Wi}});\mathbb{V}(\boldsymbol{K}_{\boldsymbol{x}_{Wi}}^{\boldsymbol{h}_{p_{Wi}}});\mathbb{V}(\boldsymbol{K}_{\boldsymbol{\omega}_i}^{\boldsymbol{h}_{p_{Wi}}});\\ &\mathbb{V}(\boldsymbol{K}_{\boldsymbol{x}_{Wi}}^{\boldsymbol{h}_{q_{Wi}}});\mathbb{V}(\boldsymbol{K}_{\boldsymbol{\omega}_i}^{\boldsymbol{h}_{q_{Wi}}});\boldsymbol{0}],\ i\in\mathcal{V}_W;\end{aligned} \tag{13b}$$

$$\begin{aligned}[\boldsymbol{\gamma}_i^b(0);\boldsymbol{\varpi}_i^b(0)] = [&\mathbb{V}(\boldsymbol{K}_{\boldsymbol{\theta}_i}^{\boldsymbol{f}_{Li}});\mathbb{V}(\boldsymbol{K}_{\boldsymbol{x}_{Li}}^{\boldsymbol{f}_{Li}});\mathbb{V}(\boldsymbol{K}_{\boldsymbol{x}_{Li}}^{\boldsymbol{h}_{p_{Li}}});\\ &\mathbb{V}(\boldsymbol{K}_{\boldsymbol{\omega}_i}^{\boldsymbol{h}_{p_{Li}}});\mathbb{V}(\boldsymbol{K}_{\boldsymbol{\omega}_i}^{\boldsymbol{h}_{q_{Li}}});\boldsymbol{0}],\ i\in\mathcal{V}_L;\end{aligned} \tag{13c}$$

$$[\boldsymbol{\gamma}_i^b(0);\boldsymbol{\varpi}_i^b(0)] = [\boldsymbol{0}],\ i\in\mathcal{V}_T. \tag{13d}$$

The designed update process (11) can be realized in a distributed manner via the communication network $\mathcal{G}_1 = \{\mathcal{V},\mathcal{E}\}$ mentioned earlier since

1. the initial values of vectors $\boldsymbol{\gamma}_i^a(0)$, $\boldsymbol{\varpi}_i^a(0)$, $\boldsymbol{\gamma}_i^b(0)$, and $\boldsymbol{\varpi}_i^b(0)$ can be assigned locally for each bus i, because i) the vectors $\boldsymbol{\gamma}_i^a(0)$, $\boldsymbol{\varpi}_i^a(0)$ can be assigned locally as each bus knows its own bus number and ii) the elements of vectors $\boldsymbol{\gamma}_i^b(0)$, $\boldsymbol{\varpi}_i^b(0)$ are obtained from the local Jacobian matrices (see (13) for details), which can be calculated based on the local steady-state measurements of θ_i, v_i, p_i^{inj}, q_i^{inj}, and state variables related to its local device or load (i.e., $\boldsymbol{x}_{Gi}$, $\boldsymbol{x}_{Wi}$, and $\boldsymbol{x}_{Li}$) since each bus is assumed to know the parameters and model structures of its local device or load [17, 18]. Here, the steady-state measurements are used to replace the calculation of the equilibrium point [14].
2. for each sub-matrix $\boldsymbol{J}_{\boldsymbol{\theta}}^{\boldsymbol{h}_p}$, $\boldsymbol{J}_{\boldsymbol{v}}^{\boldsymbol{h}_p}$, $\boldsymbol{J}_{\boldsymbol{\theta}}^{\boldsymbol{h}_q}$, $\boldsymbol{J}_{\boldsymbol{v}}^{\boldsymbol{h}_q}$ of $\boldsymbol{J}_{pf}$ (refer to (52)), the nonzero elements of the i^{th} row are functions of measurements of bus i and its neighboring bus $j\in\mathcal{N}_i$ [23, 14].

During the update process, at each step $\tau,\ 0<\tau\le 2N$, each damping bus $i,\ i\in\mathcal{V}_W\cup\mathcal{V}_L$ stores its own data and data from its neighboring buses (which can be realized via communication links between neighboring buses). Thus, the whole distributed algorithm is expressed as:

$$\begin{aligned}&[\boldsymbol{X}^a(\tau+1),\boldsymbol{X}^b(\tau+1)] = \boldsymbol{J}_{pf}[\boldsymbol{X}^a(\tau),\boldsymbol{X}^b(\tau)]\\ &[\boldsymbol{\xi}_i^a(\tau),\boldsymbol{\xi}_i^b(\tau)] = \boldsymbol{S}_i[\boldsymbol{X}^a(\tau),\boldsymbol{X}^b(\tau)],\ i\in\mathcal{V}_W\cup\mathcal{V}_L\end{aligned} \tag{14}$$

where the matrix $\boldsymbol{S}_i=[\boldsymbol{e}_i,\boldsymbol{e}_j,\boldsymbol{e}_{N+i},\boldsymbol{e}_{N+j}]^T\in\mathbb{R}^{2(\mathcal{D}_i+1)\times 2N}$, $j\in\mathcal{N}_i$ selects the rows with respect to the damping bus i and its neighboring buses $j,\ j\in\mathcal{N}_i$; $\boldsymbol{\xi}_i^a(\tau),\ \boldsymbol{\xi}_i^b(\tau)\in\mathbb{R}^{2(\mathcal{D}_i+1)\times 2N}$ denote the data collected by the damping bus i. We assume the discrete-time system (14) is observable, which usually holds in practice [14], i.e., $rank(\boldsymbol{O}_i)=2N$ where $\boldsymbol{O}_i\in\mathbb{R}^{4(\mathcal{D}_i+1)N\times 2N}$ is defined as

$$\boldsymbol{O}_i=[\boldsymbol{S}_i^T,(\boldsymbol{S}_i\boldsymbol{J}_{pf})^T,\ldots,(\boldsymbol{S}_i\boldsymbol{J}_{pf}^{2N-1})^T]^T. \tag{15}$$

After the update process (14), each damping bus $i,\ i\in\mathcal{V}_W\cup\mathcal{V}_L$ can recover $\boldsymbol{J}_{pf}$ and $\boldsymbol{X}^b(0)$ via the data it collected $\boldsymbol{\xi}_i^a(\tau)$ and $\boldsymbol{\xi}_i^b(\tau),\ \tau=0,1,\ldots,2N$. For simplicity, we define the following data matrices:

$$\begin{aligned}\boldsymbol{\Xi}_{i1}^a &= [\boldsymbol{\xi}_i^a(0)^T,\ldots,\boldsymbol{\xi}_i^a(2N-1)^T]^T\in\mathbb{R}^{4(\mathcal{D}_i+1)N\times 2N}\\ \boldsymbol{\Xi}_{i2}^a &= [\boldsymbol{\xi}_i^a(1)^T,\ldots,\boldsymbol{\xi}_i^a(2N)^T]^T\in\mathbb{R}^{4(\mathcal{D}_i+1)N\times 2N}\\ \boldsymbol{\Xi}_i^a &= [\boldsymbol{\Xi}_{i1}^{a\ T},\boldsymbol{\Xi}_{i2}^{a\ T}]^T\in\mathbb{R}^{8(\mathcal{D}_i+1)N\times 2N}\\ \boldsymbol{\Xi}_{i1}^b &= [\boldsymbol{\xi}_i^b(0)^T,\ldots,\boldsymbol{\xi}_i^b(2N-1)^T]^T\in\mathbb{R}^{4(\mathcal{D}_i+1)N\times 2N}.\end{aligned} \tag{16}$$

The singular value decomposition of $\boldsymbol{\Xi}_i^a$ is also needed, which is given as:

$$\boldsymbol{\Xi}_i^a=[\tilde{\boldsymbol{U}}_{\xi_i},\tilde{\boldsymbol{U}}_{\xi_i}^0]\begin{bmatrix}\boldsymbol{\Sigma}_{\xi_i}\\ \boldsymbol{0}\end{bmatrix}\tilde{\boldsymbol{V}}_{\xi_i}^T=\tilde{\boldsymbol{U}}_{\xi_i}\boldsymbol{\Sigma}_{\xi_i}\tilde{\boldsymbol{V}}_{\xi_i}^T \tag{17}$$

where $\boldsymbol{\Sigma}_{\xi_i},\ \tilde{\boldsymbol{V}}_{\xi_i}\in\mathbb{R}^{2N\times 2N}$, $\tilde{\boldsymbol{U}}_{\xi_i}\in\mathbb{R}^{8(\mathcal{D}_i+1)N\times 2N}$, $\tilde{\boldsymbol{U}}_{\xi_i}^0\in\mathbb{R}^{8(\mathcal{D}_i+1)N\times(8(\mathcal{D}_i+1)N-2N)}$. Based on the matrices given in (16) and (17), each damping bus $i,\ i\in\mathcal{V}_W\cup\mathcal{V}_L$ can recover $\boldsymbol{J}_{pf}$ and $\boldsymbol{X}^b(0)$ by the following equations:

$$\boldsymbol{J}_{pf}=(\tilde{\boldsymbol{U}}_{\xi_{i1}}^T\boldsymbol{\Xi}_{i1}^a)^{-1}\Theta_i\tilde{\boldsymbol{U}}_{\xi_{i1}}^T\boldsymbol{\Xi}_{i1}^a \tag{18a}$$

$$\boldsymbol{X}^b(0)=(\boldsymbol{\Xi}_{i1}^a)^\dagger\boldsymbol{\Xi}_{i1}^b \tag{18b}$$

where $\tilde{\boldsymbol{U}}_{\xi_{i1}},\ \tilde{\boldsymbol{U}}_{\xi_{i2}}\in\mathbb{R}^{4(\mathcal{D}_i+1)N\times 2N}$ are sub-matrices of $\tilde{\boldsymbol{U}}_{\xi_i}$ with $\tilde{\boldsymbol{U}}_{\xi_i}=[\tilde{\boldsymbol{U}}_{\xi_{i1}}^T,\tilde{\boldsymbol{U}}_{\xi_{i2}}^T]^T$, $\Theta_i=(\tilde{\boldsymbol{U}}_{\xi_{i1}}^T\tilde{\boldsymbol{U}}_{\xi_{i2}})(\tilde{\boldsymbol{U}}_{\xi_{i1}}^T\tilde{\boldsymbol{U}}_{\xi_{i1}})^{-1}\in\mathbb{R}^{2N\times 2N}$, and the superscript † denotes the Moore-Penrose inverse. The mathematical proof of (18a)-(18b) can be found in [14].

As mentioned earlier, each damping bus is assumed to know the model structures of SG, WTG, and load. Thus, each damping bus can identify the type of bus i (i.e, SG, WTG, load, or transfer bus) based on the $\boldsymbol{\gamma}_i^b(0)$ and $\varpi_i^b(0)$ of $\boldsymbol{X}^b(0)$ obtained, and hence can recover all $\boldsymbol{K}_\vee^\wedge$ Jacobian matrices in $\boldsymbol{K}_1$, $\boldsymbol{K}_2$, and $\boldsymbol{K}_3$ of (10) from $\boldsymbol{X}^b(0)$ obtained based on (13). Combined with $\boldsymbol{J}_{pf}$ obtained, each damping bus can reconstruct $\boldsymbol{A}_r$ by (9) and (10). Therefore, the critical LFO can be calculated by applying eigenvalue analysis to $\boldsymbol{A}_r$ at each damping bus.

Remark 2. *In the proposed update process (14), we assume that the sum of the length of all vectorized $\boldsymbol{K}_\vee^\wedge$ matrices related to each type of bus (i.e., SG, WTG, load, or transfer bus) is less than the length of the data vectors $[\boldsymbol{\gamma}_i^b;\boldsymbol{\varpi}_i^b],\ i\in\mathcal{V}$ assigned for each type of bus that is*

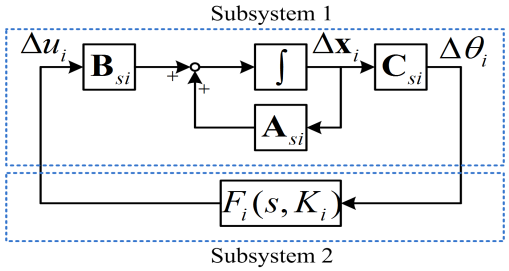

Figure 4: The closed-loop representation of the system.

$4N$ *(refer to (13) for details). If there exist one type of bus whose sum of the length of all vectorized* $\boldsymbol{K}_{\heartsuit}^{\diamondsuit}$ *matrices is more than* $4N$*, additional data vectors* $\boldsymbol{\gamma}_i^c$*,* $\boldsymbol{\varpi}_i^c \in \mathbb{R}^{2N}$ *are assigned for each bus to form the additional data matrix* $\boldsymbol{X}^c \in \mathbb{R}^{2N\times 2N}$*. For the type of bus whose sum of the length of all the vectorized* $\boldsymbol{K}_{\heartsuit}^{\diamondsuit}$ *matrices is more than* $4N$*,* $[\boldsymbol{\gamma}_i^c(0); \boldsymbol{\varpi}_i^c(0)]$ *is initialized by the remaining elements. For the other types of buses whose sum of the length of the vectorized* $\boldsymbol{K}_{\heartsuit}^{\diamondsuit}$ *matrices is less than* $4N$*,* $[\boldsymbol{\gamma}_i^c(0); \boldsymbol{\varpi}_i^c(0)]$ *is initialized by zeros. The additional data matrix* $\boldsymbol{X}^c(0)$ *can be recovered by each damping bus via the same way as the data matrix* $\boldsymbol{X}^b(0)$ *is recovered.*

3.2. Controller parameters tuning module

In order to guarantee an adequate stability margin, the damping ratio ς_c of the critical LFO $\lambda_c = \sigma_c + j\omega_c$ should satisfy $\varsigma_c \geq \varsigma^\star$ where $\varsigma_c = -\sigma_c/|\lambda_c|$ and $\varsigma^\star > 0$ is the preset threshold. Once the damping ratio of the critical LFO is less than $\varsigma^\star$, the parameters of each DCU (i.e., K_i, T_{1i}, T_{2i}, T_{3i}, and T_{4i}) of each damping bus will be tuned coordinately to improve the damping ratio of the critical LFO.

Without loss of generality, we firstly study the impact of the parameter changes of the i^{th}, $i \in \mathcal{V}_W \cup \mathcal{V}_L$ DCU (i.e., the DCU of the bus $N_G + i$) on λ_c. For analysis purposes, the system model (8) is rewritten in the following form by reordering the variables of $\boldsymbol{x}$ in (8):

$$\begin{bmatrix} \Delta\dot{\tilde{\boldsymbol{x}}}_i \\ \hdashline \mathbf{0} \end{bmatrix} = \begin{bmatrix} \tilde{\boldsymbol{A}}_{si} & \tilde{\boldsymbol{B}}_{si} \\ \hdashline \tilde{\boldsymbol{C}}_{si} & \tilde{\boldsymbol{D}}_{si} \end{bmatrix} \begin{bmatrix} \Delta\tilde{\boldsymbol{x}}_i \\ \hdashline \Delta\boldsymbol{y} \end{bmatrix} \tag{19}$$

where $\Delta\tilde{\boldsymbol{x}}_i = [\Delta\boldsymbol{x}_i^T, \Delta\boldsymbol{x}_{Ci}^T]^T$, $\boldsymbol{x}_i \in \mathbb{R}^{N_A-3}$ includes all state variables in $\boldsymbol{x}$ except $\boldsymbol{x}_{Ci} \in \mathbb{R}^3$ that is the corresponding state of the i^{th} DCU; $\tilde{\boldsymbol{A}}_{si} = \boldsymbol{T}_i^{-1}\boldsymbol{A}_s\boldsymbol{T}_i$ (here $\boldsymbol{T}_i \in \mathbb{R}^{N_A\times N_A}$ is invertable which is the corresponding elementary row operator such that $\boldsymbol{x} = \boldsymbol{T}_i\tilde{\boldsymbol{x}}_i$); $\tilde{\boldsymbol{B}}_{si} = \boldsymbol{T}_i^{-1}\boldsymbol{B}_s$; $\tilde{\boldsymbol{C}}_{si} = \boldsymbol{C}_s\boldsymbol{T}_i$; and $\tilde{\boldsymbol{D}}_{si} = \boldsymbol{D}_s$. Then the system model (19) can be written in the closed-loop form [24]. In the closed-loop form, the system model is partitioned into two subsystems. For subsystem 1, which does not depend on parameters of the i^{th} DCU, we have the following state space description:

$$\begin{bmatrix} \Delta\dot{\boldsymbol{x}}_i \\ \hdashline \mathbf{0} \end{bmatrix} = \begin{bmatrix} \boldsymbol{A}_i & \boldsymbol{B}_i \\ \hdashline \boldsymbol{C}_i & \boldsymbol{D}_i \end{bmatrix} \begin{bmatrix} \Delta\boldsymbol{x}_i \\ \hdashline \Delta\boldsymbol{y} \end{bmatrix} + \begin{bmatrix} \boldsymbol{E}_i \\ \hdashline \boldsymbol{F}_i \end{bmatrix} \Delta u_i. \tag{20}$$

where $u_i = p_{osci}$ is the output of the i^{th} DCU. Assuming $\boldsymbol{D}_i$ is nonsingular and eliminating $\Delta\boldsymbol{y}$ in (20) gives:

$$\Delta\dot{\boldsymbol{x}}_i = \boldsymbol{A}_{si}\Delta\boldsymbol{x}_i + \boldsymbol{B}_{si}\Delta u_i;\ \Delta\theta_i = \boldsymbol{C}_{si}\Delta\boldsymbol{x}_i \tag{21}$$

where $\boldsymbol{A}_{si} = \boldsymbol{A}_i - \boldsymbol{B}_i\boldsymbol{D}_i^{-1}\boldsymbol{C}_i \in \mathbb{R}^{(N_A-3)\times(N_A-3)}$, $\boldsymbol{B}_{si} = \boldsymbol{E}_i - \boldsymbol{B}_i\boldsymbol{D}_i^{-1}\boldsymbol{F}_i \in \mathbb{R}^{N_A-3}$ and $\boldsymbol{C}_{si}^T \in \mathbb{R}^{N_A-3}$. For subsystem 2, which only depends on the parameters of the i^{th} DCU, we have the following state space description:

$$\begin{bmatrix} \Delta\dot{\boldsymbol{x}}_{Ci} \\ \hdashline \Delta u_i \end{bmatrix} = \begin{bmatrix} \boldsymbol{A}_{Ci} & \boldsymbol{B}_{Ci} \\ \hdashline \boldsymbol{C}_{Ci} & \boldsymbol{D}_{Ci} \end{bmatrix} \begin{bmatrix} \Delta\boldsymbol{x}_{Ci} \\ \hdashline \Delta\theta_i \end{bmatrix}. \tag{22}$$

where $\boldsymbol{A}_{Ci}$, $\boldsymbol{B}_{Ci}$, $\boldsymbol{C}_{Ci}$, and $\boldsymbol{D}_{Ci}$ can be easily obtained from (1). A transfer function description for (22) is given as:

$$F_i(s, K_i) = \boldsymbol{C}_{Ci}(s\boldsymbol{I} - \boldsymbol{A}_{Ci})^{-1}\boldsymbol{B}_{Ci} + \boldsymbol{D}_{Ci} \tag{23}$$

where $K_i \in \mathbb{R}$ is the gain factor in the i^{th} DCU model. Based on (21) and (23), the schematic diagram of the closed-loop form is given in Fig. 4.

Then the sensitivity of λ_c with respect to K_i of the transfer function $F_i(s, K_i)$ is given by [24]:

$$\frac{\partial\lambda_c}{\partial K_i} = R_i \frac{\partial F_i(s, K_i)}{\partial K_i}\bigg|_{s=\lambda_c} \tag{24}$$

where $R_i = \boldsymbol{C}_{si}\boldsymbol{\phi}_{si}\boldsymbol{\psi}_{si}^T\boldsymbol{B}_{si} \in \mathbb{C}$ is the residue with respect to the critical eigenvalue λ_c; $\boldsymbol{\phi}_{si} \in \mathbb{R}^{N_A-3}$ and $\boldsymbol{\psi}_{si} \in \mathbb{R}^{N_A-3}$ are the right and left eigenvectors of λ_c, respectively. Here, $\boldsymbol{\phi}_{si}$ ($\boldsymbol{\psi}_{si}$) consists of the first $N_A - 3$ elements of $\boldsymbol{\phi}_i \in \mathbb{R}^{N_A}$ ($\boldsymbol{\psi}_i \in \mathbb{R}^{N_A}$) which is the right (left) eigenvector of λ_c with respect to $\tilde{\boldsymbol{A}}_{ri}$ that is obtained by eliminating $\Delta\boldsymbol{y}$ in (19), i.e.,

$$\tilde{\boldsymbol{A}}_{ri} = \tilde{\boldsymbol{A}}_{si} - \tilde{\boldsymbol{B}}_{si}\tilde{\boldsymbol{D}}_{si}^{-1}\tilde{\boldsymbol{C}}_{si} = \boldsymbol{T}_i^{-1}\boldsymbol{A}_r\boldsymbol{T}_i. \tag{25}$$

Combining (24) and the transfer function of DCU given in Fig. 1, the sensitivity of λ_c with respect to K_i becomes:

$$s_i = \frac{\partial\lambda_c}{\partial K_i} = R_i \cdot \frac{10\lambda_c}{1+10\lambda_c} \cdot \frac{1+T_{1i}\lambda_c}{1+T_{2i}\lambda_c} \cdot \frac{1+T_{3i}\lambda_c}{1+T_{4i}\lambda_c}. \tag{26}$$

Here, the wash-out time constant of each DCU is assumed to be 10, i.e., $T_{wi} = 10$.

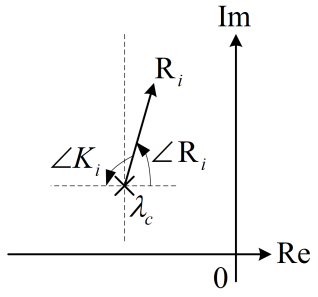

Figure 5: Representation of the residue based eigenvalue sensitivity.

Fig. 5 shows the mechanism how a residue based method changes the close loop eigenvalue. The residue R_i in (26)

is a complex number, which gives the indication of how the critical mode λ_c will be affected by the i^{th} DCU with just a gain block (no washout and lead-lag compensation blocks). In particular, the angle of the residue $\angle R_i$ gives the direction in which the root locus leaves λ_c [25, 21]. Therefore, to produce the desired damping, i.e., to make λ_c move left, the phase shift created by the i^{th} DCU should be the complement of the residue angle [25].

Based on this, it follows from (26) that the tuning process of DCUs can be split into two parts: 1) tuning parameters of lead-lag compensation of the i^{th} DCU such that $\angle s_i = 180°$; and then 2) tuning gain factors K_i of all DCUs such that λ_c moves to the desired location, i.e., $\sum_{i=1}^{N_W+N_L} |s_i|\Delta K_i \geq \Delta\Re(\lambda_c)^\star$ where $\Delta\Re(\lambda_c)^\star = \varsigma^\star|\omega_c|/\sqrt{1-(\varsigma^\star)^2} + \sigma_c$ is the expected real part change of λ_c. For part 1), the parameters of T_{1i}, T_{2i}, T_{3i}, and T_{4i} can be calculated by [26]

$$\begin{cases} \alpha_i = (1+\sin(\angle K_i)/2)/(1-\sin(\angle K_i)/2) \\ T_{1i} = T_{3i} = (\sqrt{\alpha_i})/\omega_c \\ T_{2i} = T_{4i} = 1/(\sqrt{\alpha_i}\omega_c) \end{cases} \quad (27)$$

where $\angle K_i = 180° - \angle R_i$. For part 2), the gain factor change ΔK_i is calculated by solving the following optimization problem:

$$\min \quad \sum_{i=1}^{N_W+N_L} c_i \quad (28)$$

$$\text{s.t.} \quad \sum_{i=1}^{N_W+N_L} \text{real}(s_i)\Delta K_i \geq \Delta\Re(\lambda_c)^\star \quad (29)$$

$$\Delta K_i^{min} \leq \Delta K_i \leq \Delta K_i^{max}, i = 1, \ldots, N_W + N_L \quad (30)$$

where $\text{real}(s_i)$ refers to the real part of s_i, ΔK_i^{min} and ΔK_i^{max} are the lower and upper bounds on the gain factor of the i^{th} DCU, respectively. To ensure the control accuracy, ΔK_i^{min} and ΔK_i^{max} should not be large numbers. To account for the damping controller adjustments, in this work, we introduce a simple quadratic cost function for the i^{th} damping bus which has been widely used in the literature (e.g., [12]), i.e., $c_i = \pi_i \Delta K_i^2$ and $\pi_i > 0$ is the cost parameter assigned for the i^{th} damping bus. The objective (28) is to minimize the total control cost. For convenience, the convex optimization problem (28)-(30) is rewritten in a compact form as:

$$\min_{\Delta \boldsymbol{K}} \sum_{i=1}^{N_W+N_L} c_i(\Delta K_i) \quad s.t. \;\; g(\Delta \boldsymbol{K}) \leq 0, \Delta K_i \in \Delta \hat{K}_i \quad (31)$$

where $\Delta \boldsymbol{K} = [\Delta K_1, \ldots, \Delta K_{N_W+N_L}]^T$ denotes the gain factor changes of $N_W + N_L$ DCUs; $g(\Delta \boldsymbol{K}) \leq 0$ represents the global constraint in (29); $\Delta \hat{K}_i$ represents the local constraint in (30).

As mentioned earlier, in this module, the proposed two-part tuning process will be realized in a distributed manner. For the first part tuning process, it is realized locally as the R_i required of the i^{th} damping bus can be obtained locally. It follows from (24) that R_i can be calculated by $\tilde{\boldsymbol{A}}_{ri}$, $\boldsymbol{B}_{si}$, and $\boldsymbol{C}_{si}$. For $\boldsymbol{C}_{si}$, based on (21), it can be easily obtained as the i^{th} damping bus knows the order of variables in $\boldsymbol{x}_i$. For $\tilde{\boldsymbol{A}}_{r_i}$, it can be calculated by (25) as $\boldsymbol{T}_i$ is known locally and $\boldsymbol{A}_r$ has been obtained in the critical LFO identification module for each damping bus. For $\boldsymbol{B}_{si}$, based on (19)-(22), we have

$$\tilde{\boldsymbol{A}}_{si} = \left[\begin{array}{c|c} \boldsymbol{A}_i + \boldsymbol{E}_i\boldsymbol{D}_{Ci}\boldsymbol{C}_{si} & \boldsymbol{E}_i\boldsymbol{C}_{Ci} \\ \hline \boldsymbol{B}_{Ci}\boldsymbol{C}_{si} & \boldsymbol{A}_{Ci} \end{array}\right], \; \tilde{\boldsymbol{B}}_{si} = \left[\begin{array}{c} \boldsymbol{B}_i \\ \hline \boldsymbol{0} \end{array}\right]$$
$$\tilde{\boldsymbol{C}}_{si} = \left[\begin{array}{c|c} \boldsymbol{C}_i + \boldsymbol{F}_i\boldsymbol{D}_{Ci}\boldsymbol{C}_{si} & \boldsymbol{F}_i\boldsymbol{C}_{Ci} \end{array}\right], \; \tilde{\boldsymbol{D}}_{si} = \boldsymbol{D}_i. \quad (32)$$

The $\boldsymbol{B}_{si}$ can be obtained by (21) locally as: 1) matrices $\boldsymbol{A}_{Ci}$, $\boldsymbol{B}_{Ci}$, $\boldsymbol{C}_{Ci}$, and $\boldsymbol{D}_{Ci}$ is known locally, 2) according to (19), matrices $\tilde{\boldsymbol{A}}_{si}$, $\tilde{\boldsymbol{B}}_{si}$, $\tilde{\boldsymbol{C}}_{si}$, and $\tilde{\boldsymbol{D}}_{si}$ can be calculated based on $\boldsymbol{A}_s$, $\boldsymbol{B}_s$, $\boldsymbol{C}_s$, and $\boldsymbol{D}_s$ which have been obtained by each damping bus in the critical LFO identification module, and 3) $\boldsymbol{C}_{si}$ can be obtained locally, then based on the matrix relations in (32), matrices $\boldsymbol{A}_i$, $\boldsymbol{B}_i$, $\boldsymbol{C}_i$, $\boldsymbol{D}_i$, $\boldsymbol{E}_i$, and $\boldsymbol{F}_i$ can be calculated.

For the second part tuning process, in order to solve the convex optimization problem (28)-(30) in a distributed manner, we decompose the Lagrange function of (31) into a sum of $N_W + N_L$ local Lagrange functions where each of them is assigned to a damping bus:

$$L(\Delta \boldsymbol{K}, \mu) = \sum_{i=1}^{N_W+N_L} L_i(\Delta \boldsymbol{K}, \mu) \quad (33)$$

where $L_i(\Delta \boldsymbol{K}, \mu) = c_i(\Delta K_i) + \mu g(\Delta \boldsymbol{K})$, scalar μ is the Lagrange multiplier for $g(\Delta \boldsymbol{K}) \leq 0$ in (31).

Inspired by (33), based on the distributed Lagrangian primal-dual sub-gradient algorithm proposed in [27], a distributed algorithm is designed to update the decision variables $\Delta \boldsymbol{K}$ and Lagrangian multiplier μ via communication between neighboring damping buses. The communication network used only covers damping buses and is allowed to have a different topology from the physical grid, which can be described by the undirected graph $\mathcal{G}_2 = \{\mathcal{V}_2, \mathcal{E}_2, \mathcal{W}\}$, where $\mathcal{V}_2 = \mathcal{V}_W \cup \mathcal{V}_L$, $\mathcal{E}_2 \subseteq \mathcal{V}_2 \times \mathcal{V}_2$, and $\mathcal{W} = \{w_{ij}\} \in \mathbb{R}^{(N_W+N_L)\times(N_W+N_L)}$. If $(i,j) \in \mathcal{E}_2$, $i \neq j$, then $w_{ij} = w_{ji} > 0$ and $\sum_{j=1, i\neq j}^{N_W+N_L} w_{ij} < 1$; otherwise, $w_{ij} = w_{ji} = 0$. We define the diagonal entry w_{ii} of the matrix $\mathcal{W}$ as $w_{ii} = 1 - \sum_{j=1, i\neq j}^{N_W+N_L} w_{ij}$. In the proposed distributed algorithm, the following assumptions are adopted:

1. The function g in (31) is known to all damping buses.
2. The topology of the communication network $\mathcal{G}_2$ is undirected and connected, and communication delays are negligible.

For assumption 1), since $\boldsymbol{A}_s$, $\boldsymbol{B}_s$, $\boldsymbol{C}_s$, and $\boldsymbol{D}_s$ have been obtained by each damping bus via the critical LFO identification module, then all sensitivities s_i in function g can be calculated locally for each damping bus via the same

method used for calculating R_i in the first part tuning process.

Based on the abovementioned assumptions, the update process of decision variables $\Delta \boldsymbol{K}$ and Lagrangian multiplier μ is expressed as follows:

$$\begin{aligned} \Delta \boldsymbol{K}^i(\tau+1) &= P_{\Delta \hat{K}_i}[\Delta \bar{\boldsymbol{K}}^i(\tau) - \varsigma(\tau)\mathcal{D}L_{i,\Delta \bar{\boldsymbol{K}}^i}(\tau)] \\ \mu^i(\tau+1) &= P_{\hat{U}_i}[\bar{\mu}^i(\tau) + \varsigma(\tau)\mathcal{D}L_{i,\bar{\mu}^i}(\tau)] \end{aligned} \tag{34}$$

where $\Delta \boldsymbol{K}^i \in R^{N_W+N_L}$ and $\mu^i \in R$ are the information data assigned for the i^{th} damping bus. We use $\Delta \bar{\boldsymbol{K}}^i(\tau) = \sum_{j=1}^{N_W+N_L} w_{ij}\Delta \boldsymbol{K}^j(r)$ and $\bar{\mu}^i(r) = \sum_{j=1}^{N_W+N_L} w_{ij}\mu^j(r)$ for short. At each time $\tau+1$, the i^{th} damping bus calculates vectors $\mathcal{D}L_{i,\Delta \bar{\boldsymbol{K}}^i} = \partial L_i/\partial(\Delta \bar{\boldsymbol{K}}^i)$ and $\mathcal{D}L_{i,\bar{\mu}^i} = \partial L_i/\partial \bar{\mu}^i$ in the gradient direction of its local L_i. Combined with information received from its neighboring buses $\Delta \bar{\boldsymbol{K}}^i(\tau)$ and $\bar{\mu}^i(\tau)$, the i^{th} damping bus updates its own decision variables $\Delta \boldsymbol{K}^i(\tau+1)$ and $\mu^i(\tau+1)$ by taking a projection onto its local constraint $\Delta \hat{K}_i$ and $\hat{U}_i = \{\mu_i \geq 0\}$, respectively. Here, the projection operator $P_{\Delta \hat{K}_i}$ is defined by the definition of $P_{\Delta \hat{K}_i}[\bar{\boldsymbol{x}}] = \arg\min_{\boldsymbol{x} \in \Delta \hat{K}_i} \|\bar{\boldsymbol{x}} - \boldsymbol{x}\|$, where $\bar{\boldsymbol{x}}$ is a given vector. The projection operator $P_{\hat{U}_i}$ is defined in the same way as $P_{\Delta \hat{K}_i}$. The diminishing step size is $\varsigma(r)$ which satisfies $\lim_{r \to +\infty} \varsigma(r) = 0$, $\sum_{r=0}^{+\infty} \varsigma(r) = +\infty$, and $\sum_{r=0}^{+\infty} \varsigma(r)^2 < +\infty$. It has been proven in [27] that for a convex optimization problem, the proposed distributed algorithm will asymptotically converge to a pair of primal-dual optimal solutions (i.e., $\lim_{\tau \to \infty} \Delta \boldsymbol{K}^i(\tau) = \Delta \boldsymbol{K}^*$, $i = 1, \ldots, N_W + N_L$ where $\Delta \boldsymbol{K}^* = [\Delta K_1^*, \cdots, \Delta K_{N_W+N_L}^*]^T$ is the optimal solution) under the Slater's condition, assumptions 1) and 2) mentioned above. In our case, the optimization problem (28)-(30) is a convex optimization program whose global optimal solutions can be solved in a distributed way via the algorithm (34).

It is worth mentioning that, different damping buses have different geometric controllability/obserbility measures (COs) of the critical LFO λ_c under different operating conditions [10]. The definition of the CO of the i^{th} damping bus is given as $CO_i = \frac{|\boldsymbol{\psi}_{si}^T \boldsymbol{B}_{si}|}{||\boldsymbol{\psi}_{si}||||\boldsymbol{B}_{si}||} \cdot \frac{|\boldsymbol{C}_{si}\boldsymbol{\phi}_{si}|}{||\boldsymbol{C}_{si}||||\boldsymbol{\phi}_{si}||}$ which can be calculated locally. In the proposed two-part tuning process, only the damping buses with high COs participate the tuning process. In other words, if the CO of the i^{th} damping bus satisfies $CO_i < CO^\star$ where $CO^\star$ is a threshold, then this damping bus does not participate the first part tuning process and the second part tuning process by setting $\Delta K_i^{min} = \Delta K_i^{max} = 0$ in (30) locally. In this way, the parameters needing to be tuned will be reduced by as many as possible.

The whole tuning process is summarized in the block diagram shown in Fig. 6.

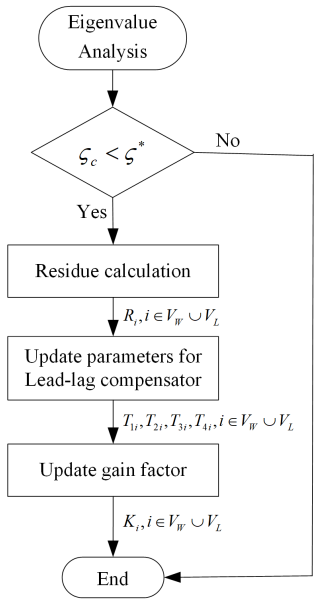

Figure 6: The flowchart of tuning procedure.

3.3. Implementation discussion

Fig. 7 illustrates the proposed online control framework, where communications between neighboring agents are required in both modules to exchange information for algorithm realization (see (14), (34), and the related discussions for details). In our assumption, communication delays are ignored. However, in practice, it is inevitable that the execution of distributed algorithms in both modules (i.e., (14) in the critical LFO identification module and (34) in the controller parameter tuning module) has latency that comes from the communication delay. Those delays can typically vary from tens to several hundreds of milliseconds [28, 29]. Considering the information update steps required in (14) and (34) ($2N$ steps for (14) and several hundred steps for (34) [6]), if we assume that the communication time required in (14) and (34) for each communication between neighboring agents are the same (e.g., 100 ms) and the delays vary from 0 to 200 ms [28], then in worst case the total communication time required for the control framework is about several minutes. Since the typical time duration for a certain load and generation pattern varies from 10 to 15 minutes [30], the time delay may not have a noticeable influence on the control performance. However, if the proposed control framework is applied to a huge system where there are several thousand buses, the impact of time delay cannot be ignored. This issue deserves attention and will be studied in future.

In the proposed control framework, we also assume that the communication link between neighboring agents provides perfect services, which is a common assumption used for distributed algorithms proposed in the literature (see [5, 14] for examples). However, communication failures may happen in practice. For the distributed algorithm (14) in the critical LFO identification module, as shown in Fig. 7, its communication network has the same structure as the power grid since each bus needs to communicate with its physically neighbouring buses. This structure is not immune to a communication link failure or a change

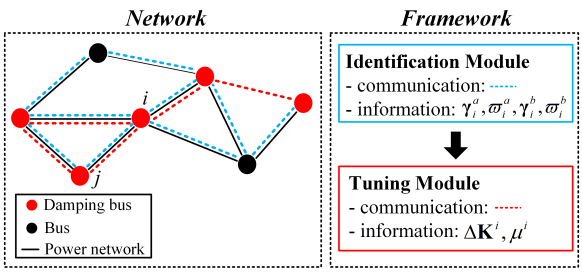

Figure 7: Diagram of control framework.

of communication network topology [14]. To solve this issue, some more reliable communication schemes can be adopted. For example, each bus can send information to its neighbours via a wired architecture such as power line communication [31]. How to develop an alternative algorithm of (14) that can survive a communication link failure or the change of communication network topology deserves attention and will be studied in future. While for distributed algorithm (34) in the controller parameter tuning module, it always works as long as the communication network is connected even if a communication link fails or a change of communication network topology occurs [27].

Remark 3. *In order to show the control effectiveness of the proposed damping controller, as mentioned earlier, the PSSs are not included in the system model. But it should be noted that the proposed control algorithm can be easily extended to incorporate PSSs in the network by regarding buses with PSSs as new damping buses since the PSS shares the similar control structure with the proposed DCU. New damping buses can take part in the proposed control framework as long as they have the ability of data processing and communicating with at least one existed damping buses. It should also be noted that the proposed control algorithm can be extended to handle the scenario where there are several critical modes (both local and inter-area ones). In this case, the tuning process can be conducted sequentially for each critical mode. This design is reasonable since the most effective damping buses (damping buses with high COs) for different critical modes are usually different, whose effectiveness is verified in the case study.*

4. Case Study

In this section, the modified 10-machine New England system and 14-generator model of the SE Australian power system are used to show the effectiveness of the proposed control framework. For each test system, the model description is introduced firstly, then, the simulation results and explanations will be presented.

4.1. 10-machine New England system

4.1.1. System description

Fig. 8 shows the modified 10-machine New England system that is used to demonstrate the proposed distributed

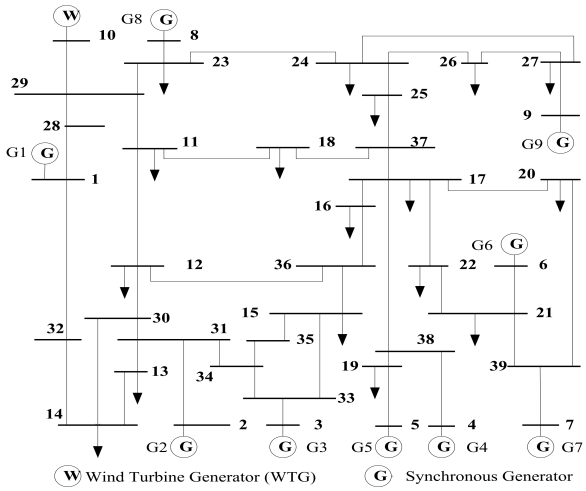

Figure 8: The modified 10-machine New England system.

control framework. In the modified system, the SG at bus 10 is replaced by a FRC-WTG with the same size of maximum power generation. All buses are renumbered according to the rules described in Section 2.2, i.e., $N_G = 9$, $N_W = 1$, $N_L = 17$, and $N_T = 12$. The damping buses considered are 1 WTG bus and 17 load buses. The model and system parameters are taken from [32]. For model parameters that are not provided in [32], we use the default values of models given in the library developed in PSAT/MATLAB, which are typical values used in dynamic simulations [33] and also verified by the case study.

For the communication network $\mathcal{G}_2$ used in the control parameters tuning module for realizing algorithm (34) (see (34) for details), each edge is assigned a weight w_{ij} that is the element of a doubly stochastic matrix $\mathcal{W}$ [27]. To obtain such a matrix, a simple approach proposed in [34] is adopted, which is used in [35] and given by:

$$w_{ij} = \frac{1}{1 + \max\{\tilde{\mathcal{D}}_i, \tilde{\mathcal{D}}_j\}}, \ i \in \mathcal{V}_2, \ j \in \tilde{\mathcal{N}}_i \qquad (35)$$

where $\tilde{\mathcal{N}}_i$ defines the set of adjacent damping buses of the i^{th} damping bus with the definition of $\tilde{\mathcal{N}}_i = \{j \in \mathcal{V}_2 : (j,i) \in \mathcal{E}_2\}$ and cardinality $|\tilde{\mathcal{N}}_i| = \tilde{\mathcal{D}}_i$.

4.1.2. Simulation results

Following the procedure described in Section 3.1, the critical LFO identified by each damping bus is $-0.0476 \pm j1.7311$ with the damping ratio $\varsigma_c = 0.0275$ (the preset threshold $\varsigma^\star = 0.1$) and oscillation frequency equal to 0.275 Hz, where G2-G9 oscillate against G1 (see Fig. 12(a) and participation factors in Fig. 9 for illustration). Then, the controller parameter tuning module is activated to tune the corresponding parameters as described in Section 3.2. The price parameters needed for the optimization problem (28)-(30) are given in Table 1. In this case study, for simplicity, we assume the gain limits for DCUs are the same

Table 1: The parameters for damping controllers

Bus no.	π	$\Delta K^\star$	Bus no.	π	$\Delta K^\star$
10	0.8692	37	19	0.8524	0
11	0.9566	0	20	0.9367	60
12	0.7578	0	21	0.7306	33
13	1.2769	0	22	0.9391	0
14	0.8650	0	23	0.7993	0
15	1.3035	0	24	1.1363	0
16	1.3578	0	25	1.0443	0
17	0.9937	42	26	0.7898	0
18	1.0715	0	27	0.9862	0

(i.e. $\Delta K^{min} = -10$ and $\Delta K^{max} = 60$). It is worth mentioning that the maximal gain (i.e., the gain limit) selected for each DCU is less than the instability gain (the gain value produces instability) [36], i.e., the variation range of gain limits of DCUs is valid. To avoid an excessive interference of the normal operation of WTGs and LAs, the limits of the supplementary input p_{osc} of DCUs are assumed to vary in the range of ± 0.05 p.u.. As mentioned in Section 3.2, only the damping buses with high COs participate the tuning process. Fig. 10 shows the COs of all 18 damping buses, and the threshold $CO^\star = 10^{-4}$. It follows from Fig. 10 that buses 10, 17, 20, and 21 participate in the parameter tuning process. The obtained optimal gain factor changes are also given in Table 1. The Table 2 compares the original λ_c, expected λ_c, and the new λ_c. It can be seen from Table 2 that the critical LFO is stabilized as desired.

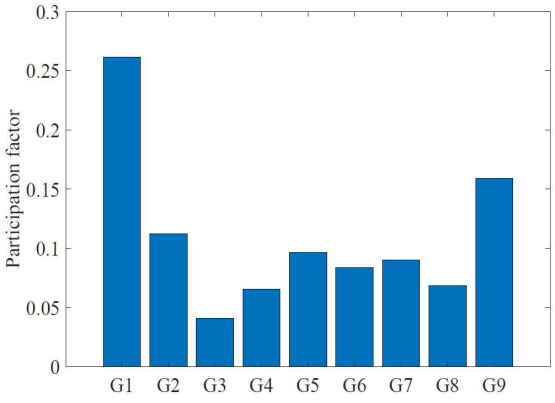

Figure 9: Participation factors of major variables related to λ_c.

Table 2: Original, expected, and new λ_c

Original λ_c	Expected λ_c	New λ_c
$-0.0476 \pm j1.7311$	$-0.1749 \pm j1.7311$	$-0.1785 \pm j1.7340$

In order to show the impact of the tuning process of DCUs on other modes (i.e., noncritical modes), Fig. 11 shows the eigenvalue profile of the system in three cases: without DCUs, with DCUs (before tuning), and with DCUs (after tuning). Here, the simple zero eigenvalue shown in Fig. 11 (and also Fig. 16) corresponds to a uniform shift $\Delta\boldsymbol{\theta} \mapsto \Delta\boldsymbol{\theta} + \alpha \mathbf{1}_N$ of all phase angle deviations $\Delta\boldsymbol{\theta}$. Since phase angle is defined only up to a synchronously rotating reference, this trivial degree of freedom can be removed by selecting one bus in the system as the angle reference bus [14]. From Fig. 11, we can see that 1) there is one critical mode and it is the inter-area mode considered, 2) the introduction of DCUs has an impact on the weak modes but will not create new weak modes, and 3) the tuning process of DCUs do not have a noticeable adverse impact on other modes.

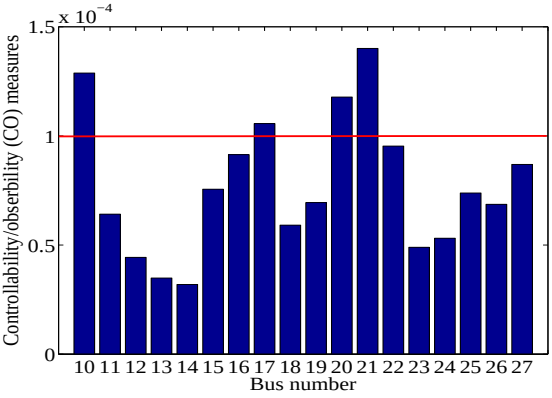

Figure 10: CO measures of all damping buses.

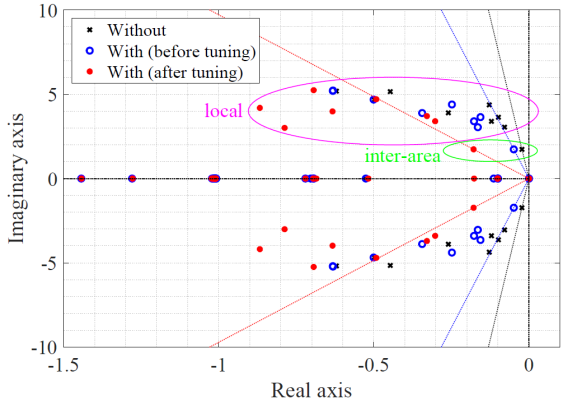

Figure 11: Eigenvalue profile of 10-machine New England system.

To illustrate the effectiveness of the proposed distributed control framework, we test the control performance with a large disturbance, i.e, a three-phase fault, which is commonly used in the literature for damping control test (see [9, 29] for examples). The variation of rotor angle of G1 after a three-phase fault before and after the proposed tuning process is investigated. The three-phase fault happens at 1 s for 0.1 seconds on bus 25. From Fig. 12(b) we can see that the system performance is improved with the

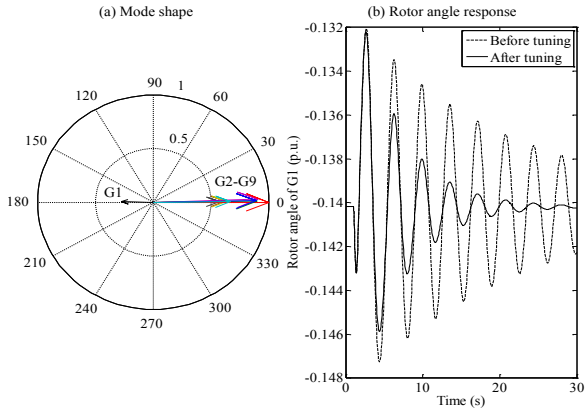

Figure 12: (a) Compass plot of relative mode shape (ref. G6) and (b) rotor angle of G1 responses to a three-phase fault on bus 25.

presence of the proposed distributed control framework. We also compare the active power injections of 4 activated damping buses (i.e., buses 10, 17, 20, and 21) during the disturbance before and after the proposed tuning process. Fig. 13 and Fig. 14 show the variation profiles of $p^{\star}_{ref}$ and p_{osc} for 4 damping buses, respectively. By comparing Fig. 13 and Fig. 14, we see that the output of DCU p_{osc} of each damping bus is very small, i.e., only a small portion of the power capacity of WTGs and LAs is required for supplementary damping control services.

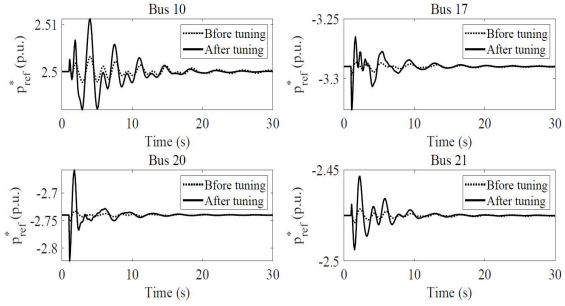

Figure 13: Variation profile of $p^{\star}_{ref}$ for damping buses.

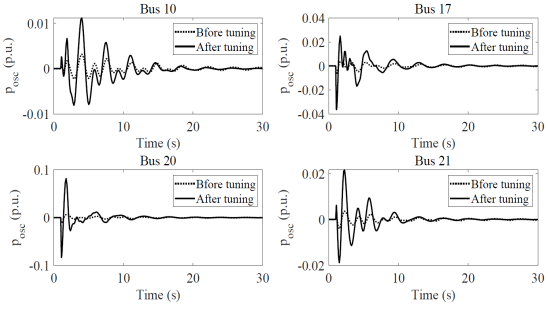

Figure 14: Variation profile of p_{osc} for damping buses.

4.2. 14-generator Australian power system

4.2.1. System description

Fig. 15 shows the modified 14-generator Australian power system [37] that is used to demonstrate the effectiveness of the proposed distributed control framework. In the modified system, the SGs at buses 203, 302, and 401 are replaced by WTGs with the same size of their maximum power generations. The damping buses considered are 3 WTG buses and 29 load buses. The model and system parameters are taken from [37]. For the parameters used in the control algorithms, they take the same settings as that used in Section 4.1.2 except the preset damping ratio threshold that is selected as $\varsigma^{\star} = 0.15$.

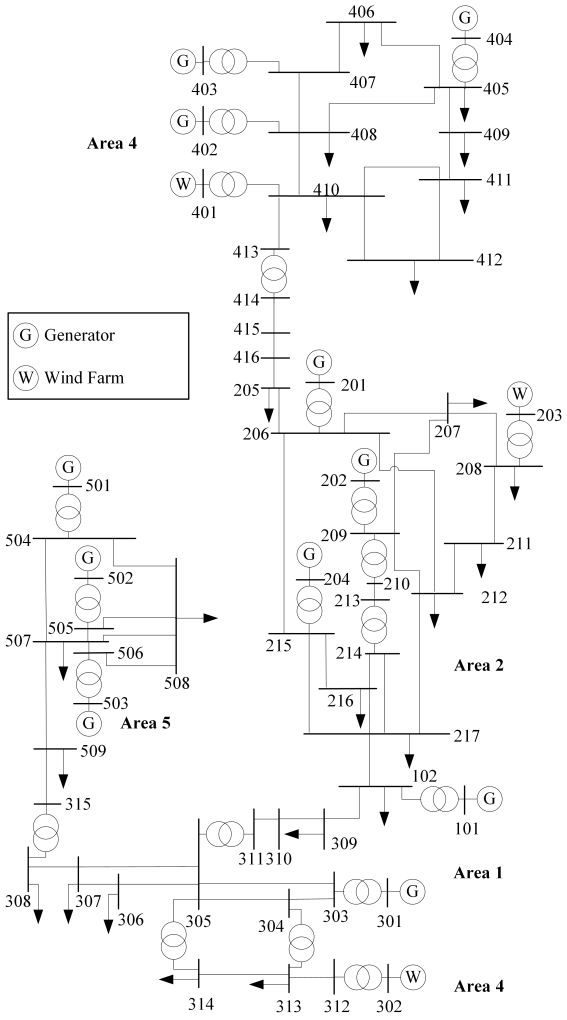

Figure 15: The modified 14-generator Australian power system.

4.2.2. Simulation results

Following the control procedure described in Section 3.1, five critical modes are detected in the system, whose damping ratio are less than 0.15 and are circled by a black ellipse in Fig. 16. It has been mentioned in Remark 3 that the proposed control approach can be extended to

handle the case where there are multiple critical modes. By implementing the parameter tuning process described in Section 3.2 on each critical mode sequentially, all critical modes are moved left, which are circled by a red ellipse in Fig. 16. The movement of critical modes shown in Fig. 16 demonstrates the effectiveness of such a tuning procedure.

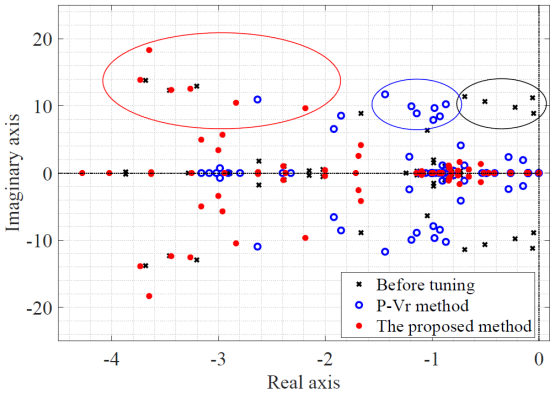

Figure 16: Eigenvalue profile of 14-generator Australian power system.

In order to show the advantage of our control approach, we compare the tuning effect of our approach with a traditional design method called P-Vr method [1]. The P-Vr method is designed in a robust fashion, i.e., a range of modal frequency is considered. In our case, the range is selected as 1.5 to 12 rad/s. The detailed tuning process of P-Vr method can be found in [37]. Fig. 16 shows the eigenvalue profile in three cases: before tuning, after tuning with P-Vr method, and after tuning with the propose approach. It can be seen from Fig. 16 that both the methods can move the critical modes left but the tuning effect of P-Vr method is not as good as that of the proposed approach. This is due to the proposed approach being able to fully exploit the control potential of controllers for a given operating condition when compared with a robust design (mentioned in Section 1).

In addition, to illustrate the effectiveness of the proposed approach, we test the system performance with a small disturbance where all active loads in Area 2 are increased by 20% at $t = 1$ s. Fig. 17 shows the frequency responses of generators in five areas, where the frequency response of one generator in each area is selected to represent the frequency behaviour of each area, dotted and solid lines refer to the cases before and after tuning with the proposed approach. From 17 we can see that the system performance is improved with the presence of the proposed distributed control framework.

5. Conclusions and future work

In this paper, with the introduction of DCU, WTGs and LAs have been coordinated to provide damping torques for the critical low frequency oscillation by adapting their

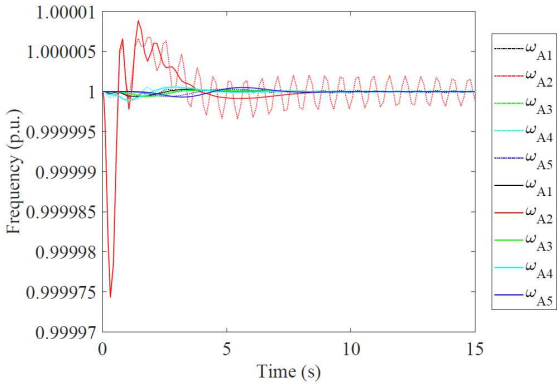

Figure 17: Frequency profile under disturbance.

active power generations and consumptions, respectively. In order to provide a scalable control framework for the increasing number of WTGs and LAs, a novel distributed control framework has been proposed, which consists of two modules: the critical LFO identification module and controller parameter tuning module. In the identification module, the system matrix required for eigenvalue analysis is reconstructed in a distributed manner. Then, based on the obtained matrix information, the parameters of DCU are tuned also in a distributed manner, which forms the second module. The simulation results have shown that the proposed distributed control framework is feasible and effective.

In the proposed control framework, communication delays are ignored in the distributed algorithms. How to cope with the communication delay and handle its impact on the control performance will be studied in future. In addition, it is assumed that communication network is reliable. An important extension is to cope with the situation where the communication link failure happens.

6. Appendix

6.1. SG model

With 4^{th}-order two-axis synchronous machine model and IEEE standard exciter model (IEEET1), the resulting differential-algebraic equations for the i^{th} SG bus are given as:

6.1.1. Differential equations

$$\dot{e}'_{qi} = \frac{1}{T'_{doi}}\left(-e'_{qi} - (x_{di} - x'_{di})i_{di} + v_{fi}\right) \tag{36a}$$

$$\dot{e}'_{di} = \frac{1}{T'_{qoi}}\left(-e'_{di} - (x_{qi} - x'_{qi})i_{qi}\right) \tag{36b}$$

$$\dot{\delta}_i = \omega_0(\omega_i - 1) \tag{36c}$$

$$\dot{\omega}_i = \frac{1}{M_i}\left(p_{mi} - e'_{di}i_{di} - e'_{qi}i_{qi} - (x'_{qi} - x'_{di})i_{di}i_{qi}\right. \quad (36d)$$

$$\left. - D_i(\omega_i - 1)\right) \quad (36e)$$

$$\dot{v}_{mi} = \frac{1}{T_{ri}}(v_i - v_{mi}) \quad (36f)$$

$$\dot{v}_{r1i} = \frac{1}{T_{ai}}\left(K_{ai}(v_{refi} - v_{mi} - v_{r2i} - \frac{K_{fi}}{T_{fi}}v_{fi}) - v_{r1i}\right) \quad (36g)$$

$$\dot{v}_{r2i} = -\frac{1}{T_{fi}}(\frac{K_{fi}}{T_{fi}}v_{fi} + v_{r2i}) \quad (36h)$$

$$\dot{v}_{fi} = -\frac{1}{T_{ei}}\left(v_{fi}(K_{ei} + S_{ei}(v_{fi}) - v_{ri})\right) \quad (36i)$$

where ω_0 is the base frequency, T'_{doi} and T'_{qoi}; x_{di} and x_{qi}; x'_{di} and x'_{qi}; i_{di} and i_{qi} are the d-axis and q-axis transient time constant; reactance; transient reactance; current, respectively; p_{mi}, D_i, and M_i are the mechanical power, damping coefficient, and moment of inertia, respectively; v_{fi} and v_{ref_i} are the field and reference voltages, respectively; T_{ri}, T_{ai}, T_{fi}, and T_{ei} are measurement, amplifier, stabilizer, and field circuit time constants, respectively; K_{ai}, K_{fi}, and K_{ei} are amplifier, stabilizer, and field circuit gains, respectively; S_{ei} is the ceiling function.

6.1.2. Algebraic equations

The stator algebraic equations are given as:

$$\begin{aligned} p_{Gi} =& i_{di}v_i\sin(\delta_i - \theta_i) + i_{qi}v_i\cos(\delta_i - \theta_i) \\ q_{Gi} =& i_{di}v_i\cos(\delta_i - \theta_i) - i_{qi}v_i\sin(\delta_i - \theta_i). \end{aligned} \quad (37)$$

In order to express network voltages in the polar form, i_{di} and i_{q_i} in (36) and (37) are expressed in terms of state variables $\boldsymbol{x}_{Gi}$ and algebraic variables v_i, θ_i:

$$\begin{bmatrix} i_{di} \\ i_{qi} \end{bmatrix} = \begin{bmatrix} r_{si} & -x'_{qi} \\ x'_{di} & r_{si} \end{bmatrix}^{-1} \begin{bmatrix} e'_{di} - v_i\sin(\delta_i - \theta_i) \\ e'_{qi} - v_i\cos(\delta_i - \theta_i) \end{bmatrix} \quad (38)$$

where r_{si} is the stator resistance. Substitution of (38) into (36) and (37) gives

$$\begin{aligned} \dot{\boldsymbol{x}}_{Gi} &= \boldsymbol{f}_{Gi}(\boldsymbol{x}_{Gi}, \theta_i, v_i) \\ p_{Gi} &= g_{p_{Gi}}(\boldsymbol{x}_{Gi}, \theta_i, v_i) \\ q_{Gi} &= g_{q_{Gi}}(\boldsymbol{x}_{Gi}, \theta_i, v_i),\ i \in \mathcal{V}_G \end{aligned} \quad (39)$$

6.2. WTG model

The model of a WTG includes models of the direct drive synchronous generator (DDSG), controller, and converter.

6.2.1. DDSG model

As the stator and rotor flux dynamics are fast in comparison with grid dynamics and the converter controls decoupled the generator from the grid, the steady-state electrical equations of DDSG are assumed. The differential and algebraic equations for DDSG of the i^{th} WTG are given as:

$$\begin{aligned} \dot{\omega}_{mi} &= \frac{1}{2H_{mi}}(\tau_{mi} - \tau_{ei}) \\ p_{si} &= v_{sdi}i_{sdi} + v_{sqi}i_{sqi} \\ q_{si} &= v_{sqi}i_{sdi} - v_{sdi}i_{sqi} \end{aligned} \quad (40)$$

with

$$\begin{aligned} \tau_{mi} &= \frac{p_{wi}(\theta_{pi})}{\omega_{mi}} \\ \tau_{ei} &= \psi_{sdi}i_{sqi} - \psi_{sqi}i_{sdi} \\ v_{sdi} &= -r_{si}i_{sdi} - \omega_{mi}\psi_{sqi} \\ v_{sqi} &= -r_{si}i_{sqi} + \omega_{mi}\psi_{sdi} \\ \psi_{sdi} &= -x_{sdi}i_{sdi} + \psi_{pmi} \\ \psi_{sqi} &= -x_{sqi}i_{sqi} \end{aligned} \quad (41)$$

where H_{mi} is the rotor inertia; $p_{wi}(\theta_{pi})$ is the mechanical power which is the function of pitch angle θ_{pi}; τ_{mi} and τ_{ei} are the mechanical and electrical torques, respectively; v_{sdi} and v_{sqi}; i_{sdi} and i_{sqi}; x_{sdi} and x_{sqi}; ψ_{sdi} and ψ_{sqi} are stator d-axis and q-axis voltages; currents; reactances; and fluxes, respectively; p_{si} and q_{si} are produced active and reactive power, respectively; r_{si} is the stator resistance; ψ_{pmi} is the permanent magnet flux of rotor. Assuming the power factor equal to 1 (permanent magnet rotor), the reactive power output of the DDSG equals zero, i.e., $q_{si} = 0$. Substituting (41) into (40) and expressing i_{sqi} with i_{sdi} based on $q_{si} = 0$ in (40) gives:

$$\begin{aligned} \dot{\omega}_{mi} &= f_{mi}(\omega_{mi}, \theta_{pi}, i_{sqi}) \\ p_{si} &= g_{spi}(i_{sqi}). \end{aligned} \quad (42)$$

6.2.2. Controller

The model of the controller includes models of the pitch angle control unit, primary frequency control unit, and the DDCU. For pitch angle control unit, its dynamic is described by the differential equation:

$$\dot{\theta}_{pi} = \frac{1}{T_{pi}}(K_{pi}\phi_i(\omega_{mi} - \omega_{mrefi}) - \theta_{pi}) \quad (43)$$

where K_{pi}, ω_{mrefi}, and T_{pi} are pitch control gain, reference rotor speed, and pitch control time constant, respectively; ϕ_i is a function which allows varying the pitch angle set point only when the difference $\omega_{mi} - \omega_{mrefi}$ exceeds a predefined value $\pm\Delta\omega_{mi}$. For the primary frequency control unit, its control is given as:

$$p_{fi} = K_{fi}(\omega_i - \omega_0) \quad (44)$$

with $\omega_i = \dot{\theta}_i$ where ω_0 is the nominal frequency and K_{fi} is the control gain. For the DDCU, its model is already given in Section 2.1 and repeated here for completeness:

$$\begin{aligned}
\dot{x}_{1i} =& -\frac{1}{T_{wi}}\left(K_i\theta_i + x_{1i}\right)\\
\dot{x}_{2i} =& \frac{1}{T_{2i}}\left((1-\frac{T_{1i}}{T_{2i}})(K_i\theta_i + x_{1i}) - x_{2i}\right)\\
\dot{x}_{3i} =& \frac{1}{T_{4i}}\left((1-\frac{T_{3i}}{T_{4i}})\left(x_{2i} + \left(\frac{T_{1i}}{T_{2i}}(K_i\theta_i + x_{1i})\right)\right) - x_{3i}\right)\\
p_{osci} =& x_{3i} + \frac{T_{3i}}{T_{4i}}\left(x_{2i} + \frac{T_{1i}}{T_{2i}}(K_i\theta_i + x_{1i})\right).
\end{aligned} \tag{45}$$

6.2.3. Converter model

Converter dynamics are highly simplified as they are fast in comparison with the electromechanical transients. Thus, the converter are modeled as an ideal current source. The differential equations for the converter of the i^{th} WTG are given as:

$$\begin{aligned}
\dot{i}_{sqi} &= \frac{1}{T_{pri}}(i_{sqrefi} - i_{sqi})\\
\dot{i}_{dci} &= \frac{1}{T_{Vi}}\left((v_{refi} - v_i) - i_{cdi}\right)
\end{aligned} \tag{46}$$

with the reference current i_{sqrefi} is defined as

$$\begin{aligned}
i_{sqrefi} =& \frac{p^{\star}_{refi}}{\omega_{mi}(\psi_{pmi} - x_{sdi}i_{sdi})}\\
=& \frac{p_{refi}(\omega_{mi}) + p_{fi} + p_{osci}}{\omega_{mi}(\psi_{pmi} - x_{sdi}i_{sdi})}
\end{aligned} \tag{47}$$

where i_{sq_i} and i_{dc_i} are state variables and are used for the active power/speed control and the reactive power/voltage control, respectively, $p_{refi}(\omega_{mi})$ is the power-speed characteristic which roughly optimizes the wind energy capture and is calculated by based on current rotor speed ω_{mi}. The active and reactive power injected into the grid from the converter are given as:

$$\begin{aligned}
p_{ci} &= v_{cdi}i_{cdi} + v_{cqi}i_{cqi}\\
q_{ci} &= v_{cqi}i_{cdi} - v_{cdi}i_{cqi}
\end{aligned} \tag{48}$$

where $v_{cdi} = -v_i\sin\theta_i$ and $v_{cqi} = v_i\cos\theta_i$.

Assuming a lossless converter, the outputs of the WTG become

$$\begin{aligned}
p_{Wi} &= p_{ci} = p_{si}\\
q_{Wi} &= v_i\left(i_{cdi}\cos\theta_i + \frac{\sin\theta_i(p_{si} + v_i i_{cdi}\sin\theta_i)}{v_i\cos\theta_i}\right).
\end{aligned} \tag{49}$$

Substituting p_{fi} in (44) and p_{osci} in (45) into (47), combining (42), (43), (45), (46), and (49) gives

$$\begin{aligned}
\dot{\theta}_i &= \omega_i\\
\dot{\boldsymbol{x}}_{Wi} &= \boldsymbol{f}_{Wi}(\boldsymbol{x}_{Wi}, \omega_i, \theta_i, v_i)\\
p_{Wi} &= g_{pW_i}(\boldsymbol{x}_{Wi}, \omega_i, \theta_i, v_i)\\
q_{Wi} &= g_{qW_i}(\boldsymbol{x}_{Wi}, \omega_i, \theta_i, v_i),\ i \in \mathcal{V}_W.
\end{aligned} \tag{50}$$

6.3. Matrices

The expression of matrices $\boldsymbol{A}_s$, $\boldsymbol{B}_s$, $\boldsymbol{C}_s$, and $\boldsymbol{D}_s$ is given in (51), where the notation $\boldsymbol{K}^{\boldsymbol{f}_i}_{\boldsymbol{x}_j}$ ($\boldsymbol{J}^{\boldsymbol{h}_i}_{\boldsymbol{x}_j}$) expresses the Jacobian matrix of the function $\boldsymbol{f}_i$ ($\boldsymbol{h}_i$) in the superscript with respect to the variable $\boldsymbol{x}_j$ in the subscript.

The expression of matrices $\boldsymbol{K}_1$, $\boldsymbol{K}_2$, $\boldsymbol{K}_3$, and $\boldsymbol{J}_{pf}$ is shown in (52), where all the Jacobian matrices $\boldsymbol{J}^{\boldsymbol{h}_i}_{\boldsymbol{x}_j}$ in (52) form the power flow Jacobian matrix $\boldsymbol{J}_{pf} \in \mathbb{R}^{2N\times 2N}$ where

$$\boldsymbol{J}_{pf} = \left[\begin{array}{c:c} \boldsymbol{J}^{\boldsymbol{h}_p}_{\boldsymbol{\theta}} & \boldsymbol{J}^{\boldsymbol{h}_p}_{\boldsymbol{v}} \\ \hdashline \boldsymbol{J}^{\boldsymbol{h}_q}_{\boldsymbol{\theta}} & \boldsymbol{J}^{\boldsymbol{h}_q}_{\boldsymbol{v}} \end{array}\right]. \tag{53}$$

The expression of matrix $\boldsymbol{T}$ is given as

$$\left[\begin{array}{cccccccccccc}
\boldsymbol{I}_{8N_G} & \boldsymbol{0} & \boldsymbol{0} & \boldsymbol{0} & \boldsymbol{0} & \boldsymbol{0} & \boldsymbol{0} & \boldsymbol{0} & \boldsymbol{0} & \boldsymbol{0} & \boldsymbol{0} & \boldsymbol{0} \\
\boldsymbol{0} & \boldsymbol{0} & \boldsymbol{0} & \boldsymbol{0} & \boldsymbol{0} & \boldsymbol{0} & \boldsymbol{I}_{N_W} & \boldsymbol{0} & \boldsymbol{0} & \boldsymbol{0} & \boldsymbol{0} & \boldsymbol{0} & \boldsymbol{0} \\
\boldsymbol{0} & \boldsymbol{0} & \boldsymbol{I}_{7N_W} & \boldsymbol{0} & \boldsymbol{0} & \boldsymbol{0} & \boldsymbol{0} & \boldsymbol{0} & \boldsymbol{0} & \boldsymbol{0} & \boldsymbol{0} & \boldsymbol{0} & \boldsymbol{0} \\
\boldsymbol{0} & \boldsymbol{0} & \boldsymbol{0} & \boldsymbol{0} & \boldsymbol{0} & \boldsymbol{0} & \boldsymbol{0} & \boldsymbol{I}_{N_L} & \boldsymbol{0} & \boldsymbol{0} & \boldsymbol{0} & \boldsymbol{0} & \boldsymbol{0} \\
\boldsymbol{0} & \boldsymbol{0} & \boldsymbol{0} & \boldsymbol{0} & \boldsymbol{I}_{3N_L} & \boldsymbol{0} & \boldsymbol{0} & \boldsymbol{0} & \boldsymbol{0} & \boldsymbol{0} & \boldsymbol{0} & \boldsymbol{0} & \boldsymbol{0} \\
\boldsymbol{0} & \boldsymbol{0} & \boldsymbol{0} & \boldsymbol{0} & \boldsymbol{0} & \boldsymbol{I}_{N_G} & \boldsymbol{0} & \boldsymbol{0} & \boldsymbol{0} & \boldsymbol{0} & \boldsymbol{0} & \boldsymbol{0} & \boldsymbol{0} \\
\boldsymbol{0} & \boldsymbol{I}_{N_W} & \boldsymbol{0} & \boldsymbol{0} & \boldsymbol{0} & \boldsymbol{0} & \boldsymbol{0} & \boldsymbol{0} & \boldsymbol{0} & \boldsymbol{0} & \boldsymbol{0} & \boldsymbol{0} & \boldsymbol{0} \\
\boldsymbol{0} & \boldsymbol{0} & \boldsymbol{0} & \boldsymbol{I}_{N_L} & \boldsymbol{0} & \boldsymbol{0} & \boldsymbol{0} & \boldsymbol{0} & \boldsymbol{0} & \boldsymbol{0} & \boldsymbol{0} & \boldsymbol{0} & \boldsymbol{0} \\
\boldsymbol{0} & \boldsymbol{0} & \boldsymbol{0} & \boldsymbol{0} & \boldsymbol{0} & \boldsymbol{0} & \boldsymbol{0} & \boldsymbol{0} & \boldsymbol{I}_{N_T} & \boldsymbol{0} & \boldsymbol{0} & \boldsymbol{0} & \boldsymbol{0} \\
\boldsymbol{0} & \boldsymbol{0} & \boldsymbol{0} & \boldsymbol{0} & \boldsymbol{0} & \boldsymbol{0} & \boldsymbol{0} & \boldsymbol{0} & \boldsymbol{0} & \boldsymbol{I}_{N_G} & \boldsymbol{0} & \boldsymbol{0} & \boldsymbol{0} \\
\boldsymbol{0} & \boldsymbol{0} & \boldsymbol{0} & \boldsymbol{0} & \boldsymbol{0} & \boldsymbol{0} & \boldsymbol{0} & \boldsymbol{0} & \boldsymbol{0} & \boldsymbol{0} & \boldsymbol{I}_{N_W} & \boldsymbol{0} & \boldsymbol{0} \\
\boldsymbol{0} & \boldsymbol{0} & \boldsymbol{0} & \boldsymbol{0} & \boldsymbol{0} & \boldsymbol{0} & \boldsymbol{0} & \boldsymbol{0} & \boldsymbol{0} & \boldsymbol{0} & \boldsymbol{0} & \boldsymbol{I}_{N_L} & \boldsymbol{0} \\
\boldsymbol{0} & \boldsymbol{0} & \boldsymbol{0} & \boldsymbol{0} & \boldsymbol{0} & \boldsymbol{0} & \boldsymbol{0} & \boldsymbol{0} & \boldsymbol{0} & \boldsymbol{0} & \boldsymbol{0} & \boldsymbol{0} & \boldsymbol{I}_{N_T}
\end{array}\right]. \tag{54}$$

7. References

References

[1] P. Kundur, N. J. Balu, M. G. Lauby, Power system stability and control, Vol. 7, McGraw-hill New York, 1994.

[2] M. Garmroodi, D. J. Hill, G. Verbič, J. Ma, Impact of tie-line power on inter-area modes with increased penetration of wind power, IEEE Transactions on Power Systems, 31 (4) (2015) 3051–3059.

[3] M. Singh, A. J. Allen, E. Muljadi, V. Gevorgian, Y. Zhang, S. Santoso, Interarea oscillation damping controls for wind power plants, IEEE Transactions on Sustainable Energy, 6 (3) (2014) 967–975.

[4] A. E. Leon, J. A. Solsona, Power oscillation damping improvement by adding multiple wind farms to wide-area coordinating controls, IEEE Transactions on Power Systems, 29 (3) (2013) 1356–1364.

[5] T. Liu, D. J. Hill, C. Zhang, Non-disruptive load-side control for frequency regulation in power systems, IEEE transactions on Smart Grid, 7 (4) (2016) 2142–2153.

[6] Z. Tang, D. J. Hill, T. Liu, H. Ma, Hierarchical voltage control of weak subtransmission networks with high penetration of wind power, IEEE Transactions on Power Systems, 33 (1) (2017) 187–197.

[7] B. Ramanathan, V. Vittal, Small-disturbance angle stability enhancement through direct load control part i-framework development, IEEE Transactions on Power Systems, 21 (2) (2006) 773–781.

[8] X. Zhang, C. Lu, S. Liu, X. Wang, A review on wide-area damping control to restrain inter-area low frequency oscillation for large-scale power systems with increasing renewable generation, Renewable and Sustainable Energy Reviews, 57 (2016) 45–58.

[9] R. A. Ramos, A. C. Martins, N. G. Bretas, An improved methodology for the design of power system damping controllers, IEEE Transactions on Power Systems, 20 (4) (2005) 1938–1945.

$$\left[\begin{array}{c:c} \boldsymbol{A}_s & \boldsymbol{B}_s \\ \hdashline \boldsymbol{C}_s & \boldsymbol{D}_s \end{array}\right] = \left[\begin{array}{ccccc:cccccccc} \boldsymbol{K}_{\boldsymbol{x}_G}^{\boldsymbol{f}_G} & \boldsymbol{0} & \boldsymbol{0} & \boldsymbol{0} & \boldsymbol{0} & \boldsymbol{K}_{\boldsymbol{\theta}_G}^{\boldsymbol{f}_G} & \boldsymbol{0} & \boldsymbol{0} & \boldsymbol{0} & \boldsymbol{K}_{\boldsymbol{v}_G}^{\boldsymbol{f}_G} & \boldsymbol{0} & \boldsymbol{0} & \boldsymbol{0} \\ \boldsymbol{0} & \boldsymbol{0} & \boldsymbol{0} & \boldsymbol{0} & \boldsymbol{0} & \boldsymbol{0} & \boldsymbol{I}_{N_W} & \boldsymbol{0} & \boldsymbol{0} & \boldsymbol{0} & \boldsymbol{0} & \boldsymbol{0} & \boldsymbol{0} \\ \boldsymbol{0} & \boldsymbol{K}_{\boldsymbol{\theta}_W}^{\boldsymbol{f}_W} & \boldsymbol{K}_{\boldsymbol{x}_W}^{\boldsymbol{f}_W} & \boldsymbol{0} & \boldsymbol{0} & \boldsymbol{0} & \boldsymbol{K}_{\boldsymbol{\omega}_W}^{\boldsymbol{f}_W} & \boldsymbol{0} & \boldsymbol{0} & \boldsymbol{0} & \boldsymbol{K}_{\boldsymbol{v}_W}^{\boldsymbol{f}_W} & \boldsymbol{0} & \boldsymbol{0} \\ \boldsymbol{0} & \boldsymbol{0} & \boldsymbol{0} & \boldsymbol{0} & \boldsymbol{0} & \boldsymbol{0} & \boldsymbol{0} & \boldsymbol{I}_{N_L} & \boldsymbol{0} & \boldsymbol{0} & \boldsymbol{0} & \boldsymbol{0} & \boldsymbol{0} \\ \boldsymbol{0} & \boldsymbol{0} & \boldsymbol{0} & \boldsymbol{K}_{\boldsymbol{\theta}_L}^{\boldsymbol{f}_L} & \boldsymbol{K}_{\boldsymbol{x}_L}^{\boldsymbol{f}_L} & \boldsymbol{0} & \boldsymbol{0} & \boldsymbol{0} & \boldsymbol{0} & \boldsymbol{0} & \boldsymbol{0} & \boldsymbol{0} & \boldsymbol{0} \\ \hdashline \boldsymbol{K}_{\boldsymbol{x}_G}^{\boldsymbol{h}_{p_G}} & \boldsymbol{J}_{\boldsymbol{\theta}_W}^{\boldsymbol{h}_{p_G}} & \boldsymbol{0} & \boldsymbol{J}_{\boldsymbol{\theta}_L}^{\boldsymbol{h}_{p_G}} & \boldsymbol{0} & \boldsymbol{J}_{\boldsymbol{\theta}_G}^{\boldsymbol{h}_{p_G}} & \boldsymbol{0} & \boldsymbol{0} & \boldsymbol{J}_{\boldsymbol{\theta}_T}^{\boldsymbol{h}_{p_G}} & \boldsymbol{J}_{\boldsymbol{v}_G}^{\boldsymbol{h}_{p_G}} & \boldsymbol{J}_{\boldsymbol{v}_W}^{\boldsymbol{h}_{p_G}} & \boldsymbol{J}_{\boldsymbol{v}_L}^{\boldsymbol{h}_{p_G}} & \boldsymbol{J}_{\boldsymbol{v}_T}^{\boldsymbol{h}_{p_G}} \\ \boldsymbol{0} & \boldsymbol{J}_{\boldsymbol{\theta}_W}^{\boldsymbol{h}_{p_W}} & \boldsymbol{K}_{\boldsymbol{x}_W}^{\boldsymbol{h}_{p_W}} & \boldsymbol{J}_{\boldsymbol{\theta}_L}^{\boldsymbol{h}_{p_W}} & \boldsymbol{0} & \boldsymbol{J}_{\boldsymbol{\theta}_G}^{\boldsymbol{h}_{p_W}} & \boldsymbol{K}_{\boldsymbol{\omega}_W}^{\boldsymbol{h}_{p_W}} & \boldsymbol{0} & \boldsymbol{J}_{\boldsymbol{\theta}_T}^{\boldsymbol{h}_{p_W}} & \boldsymbol{J}_{\boldsymbol{v}_G}^{\boldsymbol{h}_{p_W}} & \boldsymbol{J}_{\boldsymbol{v}_W}^{\boldsymbol{h}_{p_W}} & \boldsymbol{J}_{\boldsymbol{v}_L}^{\boldsymbol{h}_{p_W}} & \boldsymbol{J}_{\boldsymbol{v}_T}^{\boldsymbol{h}_{p_W}} \\ \boldsymbol{0} & \boldsymbol{J}_{\boldsymbol{\theta}_W}^{\boldsymbol{h}_{p_L}} & \boldsymbol{0} & \boldsymbol{J}_{\boldsymbol{\theta}_L}^{\boldsymbol{h}_{p_L}} & \boldsymbol{K}_{\boldsymbol{x}_L}^{\boldsymbol{h}_{p_L}} & \boldsymbol{J}_{\boldsymbol{\theta}_G}^{\boldsymbol{h}_{p_L}} & \boldsymbol{0} & \boldsymbol{K}_{\boldsymbol{\omega}_L}^{\boldsymbol{h}_{p_L}} & \boldsymbol{J}_{\boldsymbol{\theta}_T}^{\boldsymbol{h}_{p_L}} & \boldsymbol{J}_{\boldsymbol{v}_G}^{\boldsymbol{h}_{p_L}} & \boldsymbol{J}_{\boldsymbol{v}_W}^{\boldsymbol{h}_{p_L}} & \boldsymbol{J}_{\boldsymbol{v}_L}^{\boldsymbol{h}_{p_L}} & \boldsymbol{J}_{\boldsymbol{v}_T}^{\boldsymbol{h}_{p_L}} \\ \boldsymbol{K}_{\boldsymbol{x}_G}^{\boldsymbol{h}_{q_G}} & \boldsymbol{J}_{\boldsymbol{\theta}_W}^{\boldsymbol{h}_{q_G}} & \boldsymbol{0} & \boldsymbol{J}_{\boldsymbol{\theta}_L}^{\boldsymbol{h}_{q_G}} & \boldsymbol{0} & \boldsymbol{J}_{\boldsymbol{\theta}_G}^{\boldsymbol{h}_{q_G}} & \boldsymbol{0} & \boldsymbol{0} & \boldsymbol{J}_{\boldsymbol{\theta}_T}^{\boldsymbol{h}_{q_G}} & \boldsymbol{J}_{\boldsymbol{v}_G}^{\boldsymbol{h}_{q_G}} & \boldsymbol{J}_{\boldsymbol{v}_W}^{\boldsymbol{h}_{q_G}} & \boldsymbol{J}_{\boldsymbol{v}_L}^{\boldsymbol{h}_{q_G}} & \boldsymbol{J}_{\boldsymbol{v}_T}^{\boldsymbol{h}_{q_G}} \\ \boldsymbol{0} & \boldsymbol{J}_{\boldsymbol{\theta}_W}^{\boldsymbol{h}_{q_W}} & \boldsymbol{K}_{\boldsymbol{x}_W}^{\boldsymbol{h}_{q_W}} & \boldsymbol{J}_{\boldsymbol{\theta}_L}^{\boldsymbol{h}_{q_W}} & \boldsymbol{0} & \boldsymbol{J}_{\boldsymbol{\theta}_G}^{\boldsymbol{h}_{q_W}} & \boldsymbol{K}_{\boldsymbol{\omega}_W}^{\boldsymbol{h}_{q_W}} & \boldsymbol{0} & \boldsymbol{J}_{\boldsymbol{\theta}_T}^{\boldsymbol{h}_{q_W}} & \boldsymbol{J}_{\boldsymbol{v}_G}^{\boldsymbol{h}_{q_W}} & \boldsymbol{J}_{\boldsymbol{v}_W}^{\boldsymbol{h}_{q_W}} & \boldsymbol{J}_{\boldsymbol{v}_L}^{\boldsymbol{h}_{q_W}} & \boldsymbol{J}_{\boldsymbol{v}_T}^{\boldsymbol{h}_{q_W}} \\ \boldsymbol{0} & \boldsymbol{J}_{\boldsymbol{\theta}_W}^{\boldsymbol{h}_{q_W}} & \boldsymbol{0} & \boldsymbol{J}_{\boldsymbol{\theta}_L}^{\boldsymbol{h}_{q_L}} & \boldsymbol{0} & \boldsymbol{J}_{\boldsymbol{\theta}_G}^{\boldsymbol{h}_{q_L}} & \boldsymbol{0} & \boldsymbol{K}_{\boldsymbol{\omega}_L}^{\boldsymbol{h}_{q_L}} & \boldsymbol{J}_{\boldsymbol{\theta}_T}^{\boldsymbol{h}_{q_L}} & \boldsymbol{J}_{\boldsymbol{v}_G}^{\boldsymbol{h}_{q_L}} & \boldsymbol{J}_{\boldsymbol{v}_W}^{\boldsymbol{h}_{q_L}} & \boldsymbol{J}_{\boldsymbol{v}_L}^{\boldsymbol{h}_{q_L}} & \boldsymbol{J}_{\boldsymbol{v}_T}^{\boldsymbol{h}_{q_L}} \end{array}\right] \tag{51}$$

$$\left[\begin{array}{c:c} \boldsymbol{K}_1 & \boldsymbol{K}_2 \\ \hdashline \boldsymbol{K}_3 & \boldsymbol{J}_{pf} \end{array}\right] = \left[\begin{array}{ccccc:cccccccc} \boldsymbol{K}_{\boldsymbol{x}_G}^{\boldsymbol{f}_G} & \boldsymbol{0} & \boldsymbol{0} & \boldsymbol{0} & \boldsymbol{0} & \boldsymbol{K}_{\boldsymbol{\theta}_G}^{\boldsymbol{f}_G} & \boldsymbol{0} & \boldsymbol{0} & \boldsymbol{0} & \boldsymbol{K}_{\boldsymbol{v}_G}^{\boldsymbol{f}_G} & \boldsymbol{0} & \boldsymbol{0} & \boldsymbol{0} \\ \boldsymbol{0} & \boldsymbol{I}_{N_W} & \boldsymbol{0} & \boldsymbol{0} & \boldsymbol{0} & \boldsymbol{0} & \boldsymbol{0} & \boldsymbol{0} & \boldsymbol{0} & \boldsymbol{0} & \boldsymbol{0} & \boldsymbol{0} & \boldsymbol{0} \\ \boldsymbol{0} & \boldsymbol{K}_{\boldsymbol{\omega}_W}^{\boldsymbol{f}_W} & \boldsymbol{K}_{\boldsymbol{x}_W}^{\boldsymbol{f}_W} & \boldsymbol{0} & \boldsymbol{0} & \boldsymbol{0} & \boldsymbol{K}_{\boldsymbol{\theta}_W}^{\boldsymbol{f}_W} & \boldsymbol{0} & \boldsymbol{0} & \boldsymbol{0} & \boldsymbol{K}_{\boldsymbol{v}_W}^{\boldsymbol{f}_W} & \boldsymbol{0} & \boldsymbol{0} \\ \boldsymbol{0} & \boldsymbol{0} & \boldsymbol{0} & \boldsymbol{I}_{N_L} & \boldsymbol{0} & \boldsymbol{0} & \boldsymbol{0} & \boldsymbol{0} & \boldsymbol{0} & \boldsymbol{0} & \boldsymbol{0} & \boldsymbol{0} & \boldsymbol{0} \\ \boldsymbol{0} & \boldsymbol{0} & \boldsymbol{0} & \boldsymbol{0} & \boldsymbol{K}_{\boldsymbol{x}_L}^{\boldsymbol{f}_L} & \boldsymbol{0} & \boldsymbol{0} & \boldsymbol{K}_{\boldsymbol{\theta}_L}^{\boldsymbol{f}_L} & \boldsymbol{0} & \boldsymbol{0} & \boldsymbol{0} & \boldsymbol{0} & \boldsymbol{0} \\ \hdashline \boldsymbol{K}_{\boldsymbol{x}_G}^{\boldsymbol{h}_{p_G}} & \boldsymbol{0} & \boldsymbol{0} & \boldsymbol{0} & \boldsymbol{0} & \boldsymbol{J}_{\boldsymbol{\theta}_G}^{\boldsymbol{h}_{p_G}} & \boldsymbol{J}_{\boldsymbol{\theta}_W}^{\boldsymbol{h}_{p_G}} & \boldsymbol{J}_{\boldsymbol{\theta}_L}^{\boldsymbol{h}_{p_G}} & \boldsymbol{J}_{\boldsymbol{\theta}_T}^{\boldsymbol{h}_{p_G}} & \boldsymbol{J}_{\boldsymbol{v}_G}^{\boldsymbol{h}_{p_G}} & \boldsymbol{J}_{\boldsymbol{v}_W}^{\boldsymbol{h}_{p_G}} & \boldsymbol{J}_{\boldsymbol{v}_L}^{\boldsymbol{h}_{p_G}} & \boldsymbol{J}_{\boldsymbol{v}_T}^{\boldsymbol{h}_{p_G}} \\ \boldsymbol{0} & \boldsymbol{K}_{\boldsymbol{\omega}_W}^{\boldsymbol{h}_{p_W}} & \boldsymbol{K}_{\boldsymbol{x}_W}^{\boldsymbol{h}_{p_W}} & \boldsymbol{0} & \boldsymbol{0} & \boldsymbol{J}_{\boldsymbol{\theta}_G}^{\boldsymbol{h}_{p_W}} & \boldsymbol{J}_{\boldsymbol{\theta}_W}^{\boldsymbol{h}_{p_W}} & \boldsymbol{J}_{\boldsymbol{\theta}_L}^{\boldsymbol{h}_{p_W}} & \boldsymbol{J}_{\boldsymbol{\theta}_T}^{\boldsymbol{h}_{p_W}} & \boldsymbol{J}_{\boldsymbol{v}_G}^{\boldsymbol{h}_{p_W}} & \boldsymbol{J}_{\boldsymbol{v}_W}^{\boldsymbol{h}_{p_W}} & \boldsymbol{J}_{\boldsymbol{v}_L}^{\boldsymbol{h}_{p_W}} & \boldsymbol{J}_{\boldsymbol{v}_T}^{\boldsymbol{h}_{p_W}} \\ \boldsymbol{0} & \boldsymbol{0} & \boldsymbol{0} & \boldsymbol{K}_{\boldsymbol{\omega}_L}^{\boldsymbol{h}_{p_L}} & \boldsymbol{K}_{\boldsymbol{x}_L}^{\boldsymbol{h}_{p_L}} & \boldsymbol{J}_{\boldsymbol{\theta}_G}^{\boldsymbol{h}_{p_L}} & \boldsymbol{J}_{\boldsymbol{\theta}_W}^{\boldsymbol{h}_{p_L}} & \boldsymbol{J}_{\boldsymbol{\theta}_L}^{\boldsymbol{h}_{p_L}} & \boldsymbol{J}_{\boldsymbol{\theta}_T}^{\boldsymbol{h}_{p_L}} & \boldsymbol{J}_{\boldsymbol{v}_G}^{\boldsymbol{h}_{p_L}} & \boldsymbol{J}_{\boldsymbol{v}_W}^{\boldsymbol{h}_{p_L}} & \boldsymbol{J}_{\boldsymbol{v}_L}^{\boldsymbol{h}_{p_L}} & \boldsymbol{J}_{\boldsymbol{v}_T}^{\boldsymbol{h}_{p_L}} \\ \boldsymbol{K}_{\boldsymbol{x}_G}^{\boldsymbol{h}_{q_G}} & \boldsymbol{0} & \boldsymbol{0} & \boldsymbol{0} & \boldsymbol{0} & \boldsymbol{J}_{\boldsymbol{\theta}_G}^{\boldsymbol{h}_{q_G}} & \boldsymbol{J}_{\boldsymbol{\theta}_W}^{\boldsymbol{h}_{q_G}} & \boldsymbol{J}_{\boldsymbol{\theta}_L}^{\boldsymbol{h}_{q_G}} & \boldsymbol{J}_{\boldsymbol{\theta}_T}^{\boldsymbol{h}_{q_G}} & \boldsymbol{J}_{\boldsymbol{v}_G}^{\boldsymbol{h}_{q_G}} & \boldsymbol{J}_{\boldsymbol{v}_W}^{\boldsymbol{h}_{q_G}} & \boldsymbol{J}_{\boldsymbol{v}_L}^{\boldsymbol{h}_{q_G}} & \boldsymbol{J}_{\boldsymbol{v}_T}^{\boldsymbol{h}_{q_G}} \\ \boldsymbol{0} & \boldsymbol{K}_{\boldsymbol{\omega}_W}^{\boldsymbol{h}_{q_W}} & \boldsymbol{K}_{\boldsymbol{x}_W}^{\boldsymbol{h}_{q_W}} & \boldsymbol{0} & \boldsymbol{0} & \boldsymbol{J}_{\boldsymbol{\theta}_G}^{\boldsymbol{h}_{q_W}} & \boldsymbol{J}_{\boldsymbol{\theta}_W}^{\boldsymbol{h}_{q_W}} & \boldsymbol{J}_{\boldsymbol{\theta}_L}^{\boldsymbol{h}_{q_W}} & \boldsymbol{J}_{\boldsymbol{\theta}_T}^{\boldsymbol{h}_{q_W}} & \boldsymbol{J}_{\boldsymbol{v}_G}^{\boldsymbol{h}_{q_W}} & \boldsymbol{J}_{\boldsymbol{v}_W}^{\boldsymbol{h}_{q_W}} & \boldsymbol{J}_{\boldsymbol{v}_L}^{\boldsymbol{h}_{q_W}} & \boldsymbol{J}_{\boldsymbol{v}_T}^{\boldsymbol{h}_{q_W}} \\ \boldsymbol{0} & \boldsymbol{0} & \boldsymbol{0} & \boldsymbol{K}_{\boldsymbol{\omega}_L}^{\boldsymbol{h}_{q_L}} & \boldsymbol{0} & \boldsymbol{J}_{\boldsymbol{\theta}_G}^{\boldsymbol{h}_{q_L}} & \boldsymbol{J}_{\boldsymbol{\theta}_W}^{\boldsymbol{h}_{q_L}} & \boldsymbol{J}_{\boldsymbol{\theta}_L}^{\boldsymbol{h}_{q_L}} & \boldsymbol{J}_{\boldsymbol{\theta}_T}^{\boldsymbol{h}_{q_L}} & \boldsymbol{J}_{\boldsymbol{v}_G}^{\boldsymbol{h}_{q_L}} & \boldsymbol{J}_{\boldsymbol{v}_W}^{\boldsymbol{h}_{q_L}} & \boldsymbol{J}_{\boldsymbol{v}_L}^{\boldsymbol{h}_{q_L}} & \boldsymbol{J}_{\boldsymbol{v}_T}^{\boldsymbol{h}_{q_L}} \end{array}\right] \tag{52}$$

[10] Y. Zhang, A. Bose, Design of wide-area damping controllers for interarea oscillations, IEEE Transactions on Power Systems, 23 (3) (2008) 1136–1143.

[11] J. Deng, C. Li, X.-P. Zhang, Coordinated design of multiple robust facts damping controllers: A bmi-based sequential approach with multi-model systems, IEEE Transactions on Power Systems, 30 (6) (2015) 3150–3159.

[12] S. P. Azad, R. Iravani, J. E. Tate, Damping inter-area oscillations based on a model predictive control (mpc) hvdc supplementary controller, IEEE Transactions on Power Systems, 28 (3) (2013) 3174–3183.

[13] D. Fang, Y. Xiaodong, T. Chung, K. Wong, Adaptive fuzzy-logic svc damping controller using strategy of oscillation energy descent, IEEE Transactions on Power Systems, 19 (3) (2004) 1414–1421.

[14] Y. Song, D. J. Hill, T. Liu, Y. Zheng, A distributed framework for stability evaluation and enhancement of inverter-based microgrids, IEEE Transactions on Smart Grid, 8 (6) (2017) 3020–3034.

[15] L. Fan, H. Yin, Z. Miao, On active/reactive power modulation of dfig-based wind generation for interarea oscillation damping, IEEE Transactions on Energy Conversion, 26 (2) (2010) 513–521.

[16] M. E. Raoufat, K. Tomsovic, S. M. Djouadi, Dynamic control allocation for damping of inter-area oscillations, IEEE Transactions on Power Systems 32 (6) (2017) 4894–4903.

[17] P. W. Sauer, M. A. Pai, Power system dynamics and stability, Vol. 101, Prentice hall Upper Saddle River, NJ, 1998.

[18] A. Perdana, Dynamic models of wind turbines, Chalmers University of Technology, 2008.

[19] J. Morren, S. W. De Haan, W. L. Kling, J. Ferreira, Wind turbines emulating inertia and supporting primary frequency control, IEEE Transactions on power systems 21 (1) (2006) 433–434.

[20] S. Y. Hui, C. K. Lee, F. F. Wu, Electric springs—a new smart grid technology, IEEE Transactions on Smart Grid 3 (3) (2012) 1552–1561.

[21] J. Morato, T. Knüppel, J. Østergaard, Residue-based evaluation of the use of wind power plants with full converter wind turbines for power oscillation damping control, IEEE Transactions on Sustainable Energy 5 (1) (2013) 82–89.

[22] J. Soni, S. K. Panda, Electric spring for voltage and power stability and power factor correction, IEEE Transactions on Industry Applications, 53 (4) (2017) 3871–3879.

[23] Z. Tang, D. J. Hill, T. Liu, Fully distributed voltage control in subtransmission networks via virtual power plants, in: 2016 IEEE International Conference on Smart Grid Communications (SmartGridComm), IEEE, 2016, pp. 193–198.

[24] F. L. Pagola, I. J. Perez-Arriaga, G. C. Verghese, On sensitivities, residues and participations: applications to oscillatory stability analysis and control, IEEE Transactions on Power Systems, 4 (1) (1989) 278–285.

[25] G. Rogers, Power system oscillations, Springer Science & Business Media, 2012.

[26] L. Rouco, F. L. Pagola, An eigenvalue sensitivity approach to location and controller design of controllable series capacitors for damping power system oscillations, IEEE Transactions on Power Systems, 12 (4) (1997) 1660–1666.

[27] M. Zhu, S. Martínez, On distributed convex optimization under inequality and equality constraints, IEEE Transactions on

Automatic Control, 57 (1) (2011) 151–164.
[28] M. Mokhtari, F. Aminifar, D. Nazarpour, S. Golshannavaz, Wide-area power oscillation damping with a fuzzy controller compensating the continuous communication delays, IEEE Transactions on Power Systems 28 (2) (2012) 1997–2005.
[29] W. Yao, L. Jiang, J. Wen, Q. Wu, S. Cheng, Wide-area damping controller of facts devices for inter-area oscillations considering communication time delays, IEEE Transactions on Power Systems 29 (1) (2013) 318–329.
[30] T. Boehme, A. R. Wallace, G. P. Harrison, Applying time series to power flow analysis in networks with high wind penetration, IEEE transactions on power systems 22 (3) (2007) 951–957.
[31] V. C. Gungor, D. Sahin, T. Kocak, S. Ergut, C. Buccella, C. Cecati, G. P. Hancke, Smart grid technologies: Communication technologies and standards, IEEE transactions on Industrial informatics, 7 (4) (2011) 529–539.
[32] "IEEE PES Task Force on Benchmark Systems for Stability Controls," I. A. Hisken, 2013 [online]. Available: http://eioc.pnnl.gov/benchmark/ ieeess/index.htm.
[33] F. Milano, An open source power system analysis toolbox, IEEE Transactions on Power systems 20 (3) (2005) 1199–1206.
[34] L. Xiao, S. Boyd, Fast linear iterations for distributed averaging, Systems & Control Letters, 53 (1) (2004) 65–78.
[35] Z. Tang, D. J. Hill, T. Liu, A novel consensus-based economic dispatch for microgrids, IEEE Transactions on Smart Grid, 9 (4) (2018) 3920–3922.
[36] E. Larsen, D. Swann, Applying power system stabilizers part iii: Practical considerations, IEEE Transactions on Power Apparatus and Systems, (6) (1981) 3034–3046.
[37] M. Gibbard, D. Vowles, Simplified 14-generator model of the se australian power system, The University of Adelaide, South Australia (2010) 1–45.